Inertial Navigation Employing Common Frame Error Representations

Matthew P. Whittaker* and John L. Crassidis†

University at Buffalo, State University of New York, Amherst, NY 14260-4400

This paper explores a new paradigm for inertial navigation systems. Errors in filter applications using inertial navigation system equations have been previously defined from an abstract vector point-of-view. For example, the error in velocity has always been expressed using a straight difference of the truth minus the estimate without regard to each of the vector's frame representations. In this paper an alternative vector state-error is defined using common coordinates over all vector error realizations, thereby providing a true-to-life representation of the actual errors. A modified extended Kalman filter is derived that employs the alternative vector state error representation. Simulation results are shown to assess the performance of the new filter design compared with the standard inertial navigation filter.

I. Introduction

The earliest known practical application of an inertial navigation system (INS) is attributed to the German V-2 missile in 1942 [1], which employed a gyroscope, an airspeed sensor and an altimeter. A simple compass heading with a predetermined amount of fuel was used to guide the rocket to a target in a crude but effective manner. Later applications by the United States led to inertial guidance systems for ballistic missiles that could be launched from both land platforms and sea vessels. The space age brought about more accurate INS sensors, including inertial measurement units (IMUs) made up of three gyroscopes and three accelerometers mounted on a beryllium cube. Modern-day applications of INS with IMUs include aircraft navigation [2], underwater vehicles [3], and robotic systems [4].

It is well-known that all IMUs drift. For example the Apollo gyroscopes drifted about one milliradian per hour. This drift was corrected by "realigning" the inertial platform periodically through sighting on stars. This optical sighting measurements were fused with IMU data to 1) determine the drift in the IMU, and 2) propagate the inertial navigation equations using the IMU in "dynamic model replacement" mode [5] when optical sightings where not available. The workhorse for this data fusion was accomplished using the Kalman filter [6], more precisely Potter's square root extended Kalman filter (EKF) [7]. Straightforward application of the EKF for INS applications can be complicated by the choice of the attitude representation though. All minimal representations of the attitude are subject to singularity issues for certain rotations [8]. The quaternion [9] representation is now becoming mainstream because of its lack of singularity and bilinear kinematics relationship. However, handling the norm constraint is problematic. A practical solution to this problem involves using a local (minimal) error representation, such as the small angle approximation, while maintaining the quaternion as the global attitude representation. Rules of quaternion multiplication are employed in the linearization process, which maintain the norm to within the first-order approximation in the EKF. This led to the "multiplicative EKF" (MEKF) [10]. Higher-order approaches using this local/global methodology have been applied with the sigma-point Kalman filter [11], particle filter [12], as well as other filters and observers [13].

In most INS applications the state vector usually consists of the attitude, position, velocity, and IMU calibration parameters such as drifts, scale factors and misalignments. Because position-type measurements

*Graduate Research Assistant, Department of Mechanical & Aerospace Engineering. Email: mpw6@buffalo.edu. Member AIAA.

†CUBRC Professor in Space Situational Awareness, Department of Mechanical & Aerospace Engineering. Email: johnc@buffalo.edu. Fellow AIAA.

are usually only given, e.g. pseudoranges to GPS satellites, the observability of the attitude and gyroscope calibration parameters is weak, which depends on the degree of motion of the vehicle [14]. Since the early days of employing the EKF for INS applications, and even modern-day applications, the state errors are defined as a simple difference between the truth and the estimate. Reference [15] argues that a new state-error definition is required in which some state-error quantities are defined using elements expressed in a common frame, which provides a realistic framework to describe the actual errors. The errors are put into a common frame using the estimated attitude error, which led to the "geometric EKF" (GEKF). The GEKF provides extra transport terms, due to error-attitude coupling with the states, in the filter dynamics that can provide better convergence characteristics than the standard MEKF. The work in [15] focuses strictly on attitude estimation, which incorporates only "body-frame" errors. In this paper the GEKF is extended to the INS formulation. The main difference between the work in [15] and here is how errors that are expressed in some reference-frame coordinate system are handled. A complete derivation of this error is shown here, as well as simulation results that compare the standard INS EKF to the newly derived one.

The organization of this paper proceeds as follows. First a review of the quaternion kinematics is shown, followed by a review of the GEKF approach. Then, the theory behind errors expressed in reference frame coordinates is developed, which leads to a generalized theory that unified errors expressed in either body or reference frame coordinates. Then, various INS formulations of the new theory are shown using an EKF setting. Finally, conclusions are drawn based upon the developed theory and simulation results.

II. Reference Frames

In this section the reference frames used to derive the INS EKF formulations are summarized, as shown in Figure 1:

- Earth-Centered-Inertial (ECI) Frame: denoted by $\{\hat{\mathbf{i}}_1, \hat{\mathbf{i}}_2, \hat{\mathbf{i}}_3\}$. The $\hat{\mathbf{i}}_1$ axis points toward the vernal equinox direction (also known as the "First Point of Aries" or the "vernal equinox point"), the $\hat{\mathbf{i}}_3$ axis points in the direction of the North pole and the $\hat{\mathbf{i}}_2$ axis completes the right-handed system (note that the $\hat{\mathbf{i}}_1$ and $\hat{\mathbf{i}}_2$ axes are on the equator, which is the fundamental plane). The ECI frame is non-rotating with respect to the stars (except for precession of equinoxes) and the Earth turns relative to this frame. Vectors described using ECI coordinates will have a superscript I (e.g., $\mathbf{p}^I$).

- Earth-Centered-Earth-Fixed (ECEF) Frame: denoted by $\{\hat{\mathbf{e}}_1, \hat{\mathbf{e}}_2, \hat{\mathbf{e}}_3\}$. This frame is similar to the ECI frame with $\hat{\mathbf{e}}_3 = \hat{\mathbf{i}}_3$; however, the $\hat{\mathbf{e}}_1$ axis points in the direction of the Earth's prime meridian, and the $\hat{\mathbf{e}}_2$ axis completes the right-handed system. Unlike the ECI frame, the ECEF frame rotates with the Earth. The rotation angle is denoted by Θ in Figure 1. Vectors described using ECEF coordinates will have a superscript E (e.g., $\mathbf{p}^E$).

- North-East-Down (NED) Frame: denoted by $\{\hat{\mathbf{n}}, \hat{\mathbf{e}}, \hat{\mathbf{d}}\}$. This frame is used for local navigation purposes. It is formed by fitting a tangent plane to the geodetic reference ellipse at a point of interest [16]. The $\hat{\mathbf{n}}$ axis points true North, the $\hat{\mathbf{e}}$ points East, and the $\hat{\mathbf{d}}$ axis completes the right-handed system, which points in the direction of the interior of the Earth perpendicular to the reference ellipsoid. Vectors described using ECI coordinates will have a superscript N (e.g., $\mathbf{p}^N$).

- Body Frame: denoted by $\{\hat{\mathbf{b}}_1, \hat{\mathbf{b}}_2, \hat{\mathbf{b}}_3\}$. This frame is fixed onto the vehicle body and rotates with it. Conventions typically depend on the particular vehicle. Vectors described using body-frame coordinates will have a superscript B (e.g., $\mathbf{p}^B$).

The ECEF position vector is useful since this gives a simple approach to determine the longitude and latitude of a user. The Earth's geoid can be approximated by an ellipsoid of revolution about its minor axis. A common ellipsoid model is given by the World Geodetic System 1984 model (WGS-84), with semimajor axis $a = 6,378,137.0$ m and semiminor axis $b = 6,356,752.3142$ m. The eccentricity of this ellipsoid is given by $e = 0.0818$. The geodetic coordinates are given by the latitude ϕ, longitude λ and height h. To determine the ECEF position vector, the length of the normal to the ellipsoid is first computed, given by

$$N = \frac{a}{\sqrt{1 - e^2 \sin^2 \phi}} \tag{1}$$

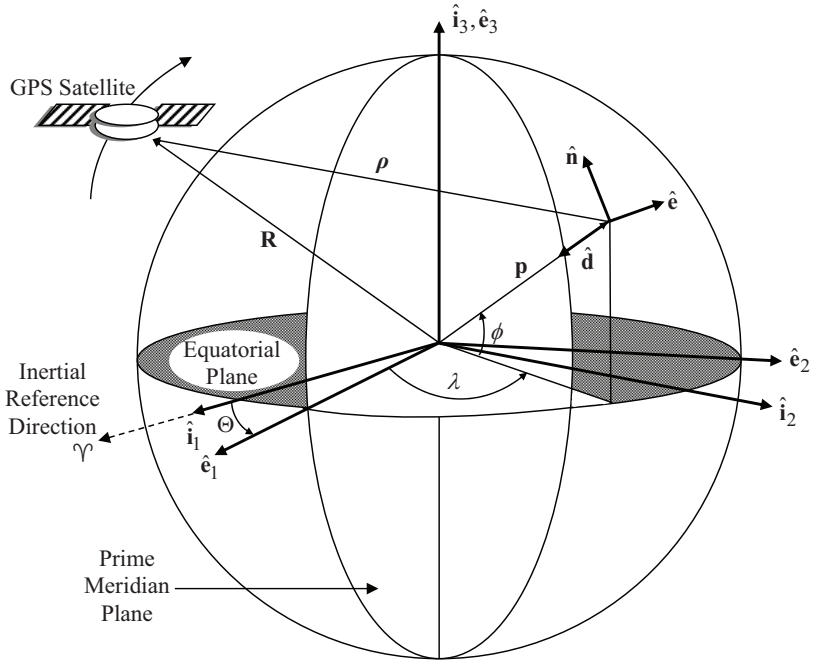

Figure 1. Definitions of Various Reference Frames

Then, given the observer geodetic quantities ϕ, λ and h, the observer ECEF position coordinates are computed using

$$x = (N + h)\cos\phi\cos\lambda \tag{2a}$$

$$y = (N + h)\cos\phi\sin\lambda \tag{2b}$$

$$z = [N(1 - e^2) + h]\sin\phi \tag{2c}$$

The conversion from ECEF to geodetic coordinates is not straightforward, but a closed-form solution is given in Ref. [18]. The conversion from ECEF coordinates to NED coordinates involves a rotation matrix from the known latitude and longitude, denoted by A_E^N. By the definition of the NED frame, a vehicle is fixed within this frame. This frame serves to define local directions for the velocity vector determined in a frame in which the vehicle has motion, such as the ECEF frame. The NED frame is generally not used to provide a vehicle's positional coordinates, but rather to provide local directions along which the velocities may be indicated. The positions are determined by relating the velocity $\mathbf{v}^N$ with the derivatives of latitude, longitude and height, and integrating the resulting equations. The attitude matrix which maps the NED frame to the vehicle body frame is denoted by A_N^B. Note that the transformation from the ECEF to the body frame is simply given by $A_E^B = A_N^B A_E^N$.

III. Quaternion Kinematics

This section provides a brief review of quaternion kinematics. For more details see Refs. [5, 9]. The attitude matrix, A, maps from the reference frame to the vehicle body frame according to $A\,\mathbf{r}$, where $\mathbf{r}$ is a component vector given with respect to the reference frame. The quaternion is a four-dimensional vector, defined as

$$\mathbf{q} \triangleq \begin{bmatrix} \boldsymbol{\varrho} \\ q_4 \end{bmatrix} \tag{3}$$

with

$$\boldsymbol{\varrho} \triangleq [q_1 \;\; q_2 \;\; q_3]^T = \mathbf{e}\sin(\vartheta/2) \tag{4a}$$

$$q_4 = \cos(\vartheta/2) \tag{4b}$$

where $\mathbf{e}$ is the unit Euler axis and ϑ is the rotation angle [9]. A quaternion parameterizing an attitude satisfies a single constraint given by $\|\mathbf{q}\| = 1$. In terms of the quaternion, its associated attitude matrix is given by

$$A(\mathbf{q}) = \Xi^T(\mathbf{q})\Psi(\mathbf{q}) \tag{5}$$

with

$$\Xi(\mathbf{q}) \triangleq \begin{bmatrix} q_4 I_{3\times 3} + [\boldsymbol{\varrho}\times] \\ -\boldsymbol{\varrho}^T \end{bmatrix}, \quad \Psi(\mathbf{q}) \triangleq \begin{bmatrix} q_4 I_{3\times 3} - [\boldsymbol{\varrho}\times] \\ -\boldsymbol{\varrho}^T \end{bmatrix} \tag{6}$$

where $I_{3\times 3}$ is a 3×3 identity matrix, and $[\boldsymbol{\varrho}\times]$ is the cross product matrix, defined by

$$[\boldsymbol{\varrho}\times] \triangleq \begin{bmatrix} 0 & -q_3 & q_2 \\ q_3 & 0 & -q_1 \\ -q_2 & q_1 & 0 \end{bmatrix} \tag{7}$$

An advantage to using quaternions is that the attitude matrix is quadratic in the parameters and also does not involve transcendental functions. For small angles the vector part of the quaternion is approximately equal to half angles so that $\boldsymbol{\varrho} \approx \boldsymbol{\alpha}/2$ and $q_4 \approx 1$, where $\boldsymbol{\alpha}$ is a vector of the roll, pitch and yaw angles. The attitude matrix can then be approximated by $A \approx I_{3\times 3} - [\boldsymbol{\alpha}\times]$ which is valid to within first-order in the angles.

Successive rotations can be accomplished using quaternion multiplication. Here we adopt the convention of Ref. [10] who multiply the quaternions in the same order as the attitude matrix multiplication (in contrast to the usual convention established by Hamiliton). A successive rotation using quaternions can be accomplished using

$$A(\mathbf{q}')A(\mathbf{q}) = A(\mathbf{q}' \otimes \mathbf{q}) \tag{8}$$

The composition of the quaternions is bilinear, with

$$\mathbf{q}' \otimes \mathbf{q} = [\Psi(\mathbf{q}') \;\; \mathbf{q}']\,\mathbf{q} = [\Xi(\mathbf{q}) \;\; \mathbf{q}]\,\mathbf{q}' \tag{9}$$

Also, the inverse quaternion is defined by

$$\mathbf{q}^{-1} \triangleq \begin{bmatrix} -\boldsymbol{\varrho} \\ q_4 \end{bmatrix} \tag{10}$$

Note that $\mathbf{q} \otimes \mathbf{q}^{-1} = [0 \;\; 0 \;\; 0 \;\; 1]^T \triangleq \mathbf{I}_q$, which is the identity quaternion.

With attitude parameterized by the quaternion $\mathbf{q}$, the physical model is then the quaternion kinematics, given by

$$\dot{\mathbf{q}} = \frac{1}{2}\Xi(\mathbf{q})\boldsymbol{\omega} = \frac{1}{2}\Omega(\boldsymbol{\omega})\mathbf{q} = \frac{1}{2}\begin{bmatrix} \boldsymbol{\omega} \\ 0 \end{bmatrix} \otimes \mathbf{q} \tag{11}$$

where $\boldsymbol{\omega} \triangleq \boldsymbol{\omega}^B_{B/I}$ is the angular velocity vector of the B frame relative to the I frame expressed in B coordinates, and

$$\Omega(\boldsymbol{\omega}) \triangleq \begin{bmatrix} -[\boldsymbol{\omega}\times] & \boldsymbol{\omega} \\ -\boldsymbol{\omega}^T & 0 \end{bmatrix} \tag{12}$$

Also, the derivative of $\mathbf{q}^{-1}$ can be shown to be given by [19]

$$\dot{\mathbf{q}}^{-1} = -\frac{1}{2}\mathbf{q}^{-1} \otimes \begin{bmatrix} \boldsymbol{\omega} \\ 0 \end{bmatrix} \tag{13}$$

The gyro measurement model is given by

$$\tilde{\boldsymbol{\omega}}^B_{B/I} = (I_{3\times 3} + \mathcal{K}_g)\boldsymbol{\omega}^B_{B/I} + \boldsymbol{\beta}_g + \boldsymbol{\eta}_{gv} \tag{14a}$$

$$\dot{\boldsymbol{\beta}}_g = \boldsymbol{\eta}_{gu} \tag{14b}$$

where $\boldsymbol{\beta}_g$ is the gyro "bias", $\mathcal{K}_g$ is a diagonal matrix of gyro scale factors, and $\boldsymbol{\eta}_{gv}$ and $\boldsymbol{\eta}_{gu}$ are zero-mean Gaussian white-noise processes with spectral densities given by $\sigma_{gv}^2 I_{3\times3}$ and $\sigma_{gu}^2 I_{3\times3}$, respectively. The accelerometer measurement model is given by

$$\tilde{\mathbf{a}}^B = (I_{3\times3} + \mathcal{K}_g)\mathbf{a}^B + \boldsymbol{\beta}_a + \boldsymbol{\eta}_{av} \tag{15a}$$

$$\dot{\boldsymbol{\beta}}_a = \boldsymbol{\eta}_{au} \tag{15b}$$

where $\boldsymbol{\beta}_a$ is the accelerometer "bias", $\mathcal{K}_a$ is a diagonal matrix of accelerometer scale factors, and $\boldsymbol{\eta}_{av}$ and $\boldsymbol{\eta}_{au}$ are zero-mean Gaussian white-noise processes with spectral densities given by $\sigma_{av}^2 I_{3\times3}$ and $\sigma_{au}^2 I_{3\times3}$, respectively. We should note that most manufacturers give values for σ_{gv} and σ_{av}, but not σ_{gu} and σ_{au}. The scale factors are assumed to be small enough so that the approximation $(I+\mathcal{K})^{-1} \approx (I-\mathcal{K})$ is valid for both the gyros and acclerometers. Simulating gyro and accelerometer using computers is not easy since continuous measurements cannot be generated using digital computers. A discrete-time simulation is possible using the spectral densities though [5]. The gyro measurement can be simulated using

$$\tilde{\omega}_{k+1} = \boldsymbol{\omega}_{k+1} + \frac{1}{2}(\boldsymbol{\beta}_{g_{k+1}} + \boldsymbol{\beta}_{g_k}) + \left(\frac{\sigma_{gv}^2}{\Delta t} + \frac{1}{12}\sigma_{gu}^2\,\Delta t\right)^{1/2} \mathbf{N}_{gv_k} \tag{16a}$$

$$\boldsymbol{\beta}_{g_{k+1}} = \boldsymbol{\beta}_{g_k} + \sigma_{gu}\,\Delta t^{1/2}\mathbf{N}_{gu_k} \tag{16b}$$

where the subscript k denotes the k^{th} time-step, Δt denotes the sampling interval, and $\mathbf{N}_{gv_k}$ and $\mathbf{N}_{gu_k}$ are zero-mean Gaussian white-noise processes with covariance each given by the identity matrix. Replacing $\boldsymbol{\omega}_{k+1}$ with $(I_3 + \mathcal{K}_g)\,\boldsymbol{\omega}_{k+1}$ in Eq. (16a) provides the discrete-time model for Eq. (14). A similar model can be employed for the discrete-time accelerometer measurement.

IV. Geometric Filtering

This section provides a review of the GEKF (more details can be found in Ref. [15]). Ideally, the appropriate filter would employ state errors between the true variables ($\mathbf{q}$, $\boldsymbol{\beta}$) and their corresponding estimates ($\hat{\mathbf{q}}$, $\hat{\boldsymbol{\beta}}$) defined by

$$\mathbf{dq} \triangleq \mathbf{q} \otimes \hat{\mathbf{q}}^{-1} \equiv \begin{bmatrix}\mathbf{d}\boldsymbol{\varrho}^T & \mathrm{d}q_4\end{bmatrix}^T \tag{17a}$$

$$\mathbf{d}\boldsymbol{\beta} \triangleq A^T(\mathbf{dq})\boldsymbol{\beta} - \hat{\boldsymbol{\beta}} \tag{17b}$$

where $\boldsymbol{\beta}$ is any state expressed in body-frame coordinates, such a strapdown gyro-bias state, and all realizations of $\mathbf{d}\boldsymbol{\beta}$ are expressed within the mean (estimated) coordinate frame. Also, $A(\mathbf{dq})$ is the attitude-error matrix that maps mean-frame quantities to their respective true frames. The first-order approximation of the attitude error-quaternion $\mathbf{dq}$ is given by $\mathbf{dq} \approx [\frac{1}{2}\mathbf{d}\boldsymbol{\alpha}^T \;\; 1]^T$ [10], where $\mathbf{d}\boldsymbol{\alpha}$ is a vector of small, roll, pitch and yaw angles for any rotation sequence. Then the rotation matrix in Eq. (17b) is approximated by

$$A(\mathbf{dq}) \equiv A(\mathbf{d}\boldsymbol{\alpha}) \approx I_{3\times3} - [\mathbf{d}\boldsymbol{\alpha}\times] \tag{18}$$

with $\mathbf{d}\boldsymbol{\alpha} = 2\,\mathbf{d}\boldsymbol{\varrho}$. Because the series expansions deriving the EKF are truncated to first-order, a linearized approximation is adequate because higher-order terms will ultimately be discarded. Thus, the error definitions are related according to

$$\mathbf{q} - \hat{\mathbf{q}} \approx \frac{1}{2}\Xi(\hat{\mathbf{q}})\mathbf{d}\boldsymbol{\alpha} \tag{19a}$$

$$\boldsymbol{\beta} - \hat{\boldsymbol{\beta}} \approx [\hat{\boldsymbol{\beta}}\times]\mathbf{d}\boldsymbol{\alpha} + \mathbf{d}\boldsymbol{\beta} \tag{19b}$$

where the approximation to the attitude matrix in Eq. (18) is used in obtaining Eq. (19b). Equation (19a) is recognized as the mapping employed by the "reduced covariance" approach to deriving the MEKF [10]. Assembling the components of Eq (19) leads to

$$\Delta\mathbf{x} \approx C\mathbf{dx} \tag{20}$$

where $\Delta\mathbf{x} \triangleq [(\mathbf{q} - \hat{\mathbf{q}})^T \ (\boldsymbol{\beta} - \hat{\boldsymbol{\beta}})^T]^T$, $\mathbf{dx} \triangleq [\mathbf{d}\boldsymbol{\alpha}^T \ \mathbf{d}\boldsymbol{\beta}^T]^T$, and the "error map" C is defined according to

$$C \triangleq \begin{bmatrix} \frac{1}{2}\Xi(\hat{\mathbf{q}}) & 0_{4\times 3} \\ [\hat{\boldsymbol{\beta}}\times] & I_{3\times 3} \end{bmatrix} \tag{21}$$

where $0_{m\times n}$ is an $m \times n$ matrix of zeros.

A. Propagation

The dynamic model is given by

$$\dot{\mathbf{x}} = \mathbf{f}(\mathbf{x}, \mathbf{w}) \tag{22}$$

where $\mathbf{x}$ is the $n \times 1$ state vector, and $\mathbf{w}$ is the zero-mean Gaussian process noise vector with spectral density given by Q. Following classical developments of the EKF, the estimated dynamics follow

$$\dot{\hat{\mathbf{x}}} = \mathbf{f}(\hat{\mathbf{x}}) \tag{23}$$

The standard EKF approximates the local dynamics with the truncated Taylor series expansion, given by

$$\dot{\mathbf{x}} \approx \mathbf{f}(\hat{\mathbf{x}}) + F_a\Delta\mathbf{x} + G_a\mathbf{w} \tag{24}$$

which is expanded about the approximate conditional mean $\hat{\mathbf{x}}$ (and about the mean process noise vector, $\hat{\mathbf{w}} = \mathbf{0}$). Also, F_a and G_a are the standard linearized state and process noise matrices, respectively. In the GEKF the standard EKF error definition $\Delta\mathbf{x}$ is replaced using the relationship of Eq. (20). The state dynamics in the GEKF are given by

$$\dot{\mathbf{x}} = \mathbf{f}(\hat{\mathbf{x}}) + F_aC\mathbf{dx} + G_a\mathbf{w} \tag{25}$$

The error dynamics in the GEKF can be shown to be given by

$$\mathbf{d}\dot{\mathbf{x}} = F_g\mathbf{dx} + G_g\mathbf{w} \tag{26}$$

where

$$F_g = (C^TC)^{-1}C^T(F_aC - \dot{C}) \tag{27a}$$

$$G_g = (C^TC)^{-1}C^TG_a \tag{27b}$$

Reference [15] proves that both F_g and G_g are unique. The GEKF error-covariance, $\mathcal{P}$, is governed by the differential equation

$$\dot{\mathcal{P}} = F_g\mathcal{P} + \mathcal{P}F_g^T + G_gQG_g^T \tag{28}$$

Equations (23) and (28) comprise the propagation stage of the GEKF algorithm.

B. Update

Consider the following discrete-time measurement:

$$\tilde{\mathbf{y}}_k = \mathbf{h}_k(\mathbf{x}_k) + \mathbf{v}_k \tag{29}$$

where $\mathbf{v}_k$ is a zero-mean Gaussian noise process with covariance R_k. Expanding $\mathbf{h}_k(\mathbf{x}_k)$ in a Taylor series about the *a priori* state estimate, $\hat{\mathbf{x}}_k^-$, and truncating to first-order leads to

$$\mathbf{h}_k(\mathbf{x}_k) \approx \mathbf{h}_k(\hat{\mathbf{x}}_k^-) + H_kC_k^-\mathbf{dx}_k^- \tag{30}$$

where $C_k^- \triangleq C(t_k^-)$ and $\mathbf{dx}_k^-$ denote the *a priori* error map and state error, respectively, and H_k is the usual EKF sensitivity matrix. The update in the GEKF is given by the usual form:

$$\hat{\mathbf{x}}_k^+ = \hat{\mathbf{x}}_k^- + K_k\left[\tilde{\mathbf{y}}_k - \mathbf{h}_k(\hat{\mathbf{x}}_k^-)\right] \tag{31}$$

The gain equation in the GEKF is different than the standard EKF though. This is given by

$$K_k = C_k^-\mathcal{P}_k^-[C_k^-]^TH_k^T\left[H_kC_k^-\mathcal{P}_k^-[C_k^-]^TH_k^T + R_k\right]^{-1} \tag{32}$$

Table 1. Geometric Extended Kalman Filter

Parameter	Value
Model	$\dot{\mathbf{x}} = \mathbf{f}[\mathbf{x}(t),\, \mathbf{w}(t)], \quad E\{\mathbf{w}(t)\mathbf{w}^T(\tau)\} = Q(t)\delta(t-\tau)$
	$\tilde{\mathbf{y}}_k = \mathbf{h}_k(\mathbf{x}_k) + \mathbf{v}_k, \quad E\{\mathbf{v}_k\mathbf{v}_k^T\} = R_k$
Initialize	$\hat{\mathbf{x}}(t_0) = \hat{\mathbf{x}}_0$
	$\mathcal{P}(t_0) = E\{\mathbf{dx}_0\, \mathbf{dx}_0^T\}$
Gain	$\bar{K}_k = \mathcal{P}_k^- \bar{H}_k^T [\bar{H}_k \mathcal{P}_k^- \bar{H}_k^T + R_k]^{-1}$
	$\bar{H}_k = H_k C_k^-$
	$H_k = \left.\dfrac{\partial \mathbf{h}}{\partial \mathbf{x}}\right\vert_{\hat{\mathbf{x}}_k^-}$
	$\Delta\mathbf{x}_k = C_k \mathbf{dx}_k$
Update	$\begin{bmatrix}\hat{\mathbf{q}}_k^+ \\ \hat{\boldsymbol{\beta}}_k^+\end{bmatrix} = \begin{bmatrix}\hat{\mathbf{q}}_k^- \\ \hat{\boldsymbol{\beta}}_k^-\end{bmatrix} + C_k^- \bar{K}_k \left[\tilde{\mathbf{y}}_k - \mathbf{h}_k(\hat{\mathbf{x}}_k^-)\right]$
	$\hat{\mathbf{q}}_k^+ \leftarrow \hat{\mathbf{q}}_k^+ / \Vert\hat{\mathbf{q}}_k^+\Vert$
	$\mathcal{P}_k^+ = \bar{M}_k \left\{[I_{(n-1)\times(n-1)} - \bar{K}_k\bar{H}_k]\mathcal{P}_k^-[I_{(n-1)\times(n-1)} - \bar{K}_k\bar{H}_k]^T + \bar{K}_k R_k \bar{K}_k^T\right\} \bar{M}_k^T$
	$\bar{M}_k \triangleq \left([C_k^+]^T C_k^+\right)^{-1} [C_k^+]^T C_k^-$
Propagation	$\dot{\hat{\mathbf{x}}} = \mathbf{f}(\hat{\mathbf{x}})$
	$\dot{\mathcal{P}} = F_g\mathcal{P} + \mathcal{P}F_g^T + G_g Q G_g^T$
	$F_g = (C^TC)^{-1}C^T(F_aC - \dot{C}), \quad G_g = (C^TC)^{-1}C^TG_a$
	$F_a = \left.\dfrac{\partial \mathbf{f}}{\partial \mathbf{x}}\right\vert_{\hat{\mathbf{x}}}, \quad G_a = \left.\dfrac{\partial \mathbf{f}}{\partial \mathbf{w}}\right\vert_{\hat{\mathbf{x}}}$

Also, the error-covariance update is different, which is given by

$$\mathcal{P}_k^+ = \bar{M}_k \left\{[I_{(n-1)\times(n-1)} - \bar{K}_k\bar{H}_k]\mathcal{P}_k^-[I_{(n-1)\times(n-1)} - \bar{K}_k\bar{H}_k]^T + \bar{K}_k R_k \bar{K}_k^T\right\} \bar{M}_k^T \tag{33}$$

where $\bar{H}_k \triangleq H_k C_k^-$ and $\bar{K}_k \triangleq \mathcal{P}_k^- \bar{H}_k^T [\bar{H}_k \mathcal{P}_k^- \bar{H}_k + R_k]^{-1}$, and the transformation $\bar{M}_k$ is given by

$$\bar{M}_k \triangleq \left([C_k^+]^T C_k^+\right)^{-1} [C_k^+]^T C_k^- \tag{34}$$

Note that as $\hat{\mathbf{x}}_k^-$ approaches $\hat{\mathbf{x}}_k^+$, the transformation $\bar{M}_k$ approaches identity. Note that the state is reduced by 1 as evident by the use of the $(n-1)\times(n-1)$ identity matrix in Eq. (33). This is due to the fact that a local (minimal) error representation is used for the attitude error, as discussed in Ref. [10]. Equations (31) and (33) define the GEKF update stage. A summary of the GEKF is shown in Table 1. It should be noted that the quaternion update arises from a multiplicative update [10], even though it can be written as an additive update, i.e. the update maintains quaternion normalization to within first order.

V. Geometric Body and Reference Frame Errors

The derivation in Ref. [15] assumes that errors exist in only the body frame, which will be shown explicitly shortly. For example, gyro biases are associated with a vehicle's body frame, and all realizations

of the stochastic errors are given with respect to this frame. However, INS applications also have errors associated with respect to some reference frame. For example, the velocity is defined with respect to a specified reference frame, and all realizations of the stochastic errors are given with respect to this frame. A complete characterization of errors in both the body frame and reference frame requires four frames: 1) True Reference R, Mean Reference $\hat{R}$, True Body B, and Mean Body $\hat{B}$. The body-frame error-quaternion is given by

$$\mathbf{dq}_B = \mathbf{q}_{BR} \otimes \mathbf{q}_{R\hat{R}} \otimes \mathbf{q}_{\hat{R}\hat{B}} \tag{35}$$

where $\mathbf{q}_{BR}$ maps from the true reference to the true body, $\mathbf{q}_{R\hat{R}}$ maps from the mean reference to the true reference, and $\mathbf{q}_{\hat{R}\hat{B}}$ maps from the mean body to the mean reference. The reference-frame error-quaternion is given by

$$\mathbf{dq}_R = \mathbf{q}_{\hat{R}\hat{B}} \otimes \mathbf{q}_{\hat{B}B} \otimes \mathbf{q}_{BR} \tag{36}$$

where $\mathbf{q}_{\hat{R}\hat{B}}$ maps from the mean body to the mean reference, $\mathbf{q}_{\hat{B}B}$ maps from the true body to the mean body, and $\mathbf{q}_{BR}$ maps from the true reference to the true body. These conventions are chosen so that if $\mathbf{q}_{R\hat{R}}$ and $\mathbf{q}_{\hat{B}B}$ are both the identity quaternions, then the error-quaternions would follow the Ref. [10] for the body-frame error, and Ref. [20] for the reference-frame error conventions directly. The true and estimated quaternions are equivalent to

$$\mathbf{q} \equiv \mathbf{q}_{BR} \tag{37a}$$

$$\hat{\mathbf{q}} \equiv \mathbf{q}_{\hat{B}\hat{R}} \tag{37b}$$

Then

$$\mathbf{dq}_B = \mathbf{q} \otimes \mathbf{dq}_R^{-1} \otimes \hat{\mathbf{q}}^{-1} \tag{38a}$$

$$\mathbf{dq}_R = \hat{\mathbf{q}}^{-1} \otimes \mathbf{dq}_B^{-1} \otimes \mathbf{q} \tag{38b}$$

and

$$\mathbf{dq}_B^{-1} = \hat{\mathbf{q}} \otimes \mathbf{dq}_R \otimes \mathbf{q}^{-1} \tag{39a}$$

$$\mathbf{dq}_R^{-1} = \mathbf{q}^{-1} \otimes \mathbf{dq}_B \otimes \hat{\mathbf{q}} \tag{39b}$$

It is now shown that these four frames are not independent of each other. This is first done by deriving the kinematics for $\mathbf{dq}_B$ and $\mathbf{dq}_R$. Taking the time derivative of the expressions in Eq. (38) gives

$$\mathbf{d\dot{q}}_B = \dot{\mathbf{q}} \otimes \mathbf{dq}_R^{-1} \otimes \hat{\mathbf{q}}^{-1} + \mathbf{q} \otimes \mathbf{d\dot{q}}_R^{-1} \otimes \hat{\mathbf{q}}^{-1} + \mathbf{q} \otimes \mathbf{dq}_R^{-1} \otimes \dot{\hat{\mathbf{q}}}^{-1} \tag{40a}$$

$$\mathbf{d\dot{q}}_R = \dot{\hat{\mathbf{q}}}^{-1} \otimes \mathbf{dq}_B^{-1} \otimes \mathbf{q} + \hat{\mathbf{q}}^{-1} \otimes \mathbf{d\dot{q}}_B^{-1} \otimes \mathbf{q} + \hat{\mathbf{q}}^{-1} \otimes \mathbf{dq}_B^{-1} \otimes \dot{\mathbf{q}} \tag{40b}$$

Taking the time derivative of the expressions in Eq. (39) gives

$$\mathbf{d\dot{q}}_B^{-1} = \dot{\hat{\mathbf{q}}} \otimes \mathbf{dq}_R \otimes \mathbf{q}^{-1} + \hat{\mathbf{q}} \otimes \mathbf{d\dot{q}}_R \otimes \mathbf{q}^{-1} + \hat{\mathbf{q}} \otimes \mathbf{dq}_R \otimes \dot{\mathbf{q}}^{-1} \tag{41a}$$

$$\mathbf{d\dot{q}}_R^{-1} = \dot{\mathbf{q}}^{-1} \otimes \mathbf{dq}_B \otimes \hat{\mathbf{q}} + \mathbf{q}^{-1} \otimes \mathbf{d\dot{q}}_B \otimes \hat{\mathbf{q}} + \mathbf{q}^{-1} \otimes \mathbf{dq}_B \otimes \dot{\hat{\mathbf{q}}} \tag{41b}$$

Substituting Eqs. (39b) and (41b) into Eq. (40a) gives

$$\mathbf{d\dot{q}}_B = \dot{\mathbf{q}} \otimes \mathbf{q}^{-1} \otimes \mathbf{dq}_B + \mathbf{q} \otimes \dot{\mathbf{q}}^{-1} \otimes \mathbf{dq}_B + \mathbf{d\dot{q}}_B + \mathbf{dq}_B \otimes \dot{\hat{\mathbf{q}}} \otimes \hat{\mathbf{q}}^{-1} + \mathbf{dq}_B \otimes \hat{\mathbf{q}} \otimes \dot{\hat{\mathbf{q}}}^{-1} \tag{42}$$

Substituting Eqs. (11) and (13), and their respective estimated quantities, given by the following kinematics relations:

$$\dot{\hat{\mathbf{q}}} = \frac{1}{2} \begin{bmatrix} \hat{\boldsymbol{\omega}} \\ 0 \end{bmatrix} \otimes \hat{\mathbf{q}} \tag{43a}$$

$$\dot{\hat{\mathbf{q}}}^{-1} = -\frac{1}{2} \hat{\mathbf{q}}^{-1} \otimes \begin{bmatrix} \hat{\boldsymbol{\omega}} \\ 0 \end{bmatrix} \tag{43b}$$

into Eq. (42) gives $\mathbf{0} = \mathbf{0}$. This clearly shows that the four frames are not independent.

Another approach provides the same conclusion. Taking the time derivative of $\mathbf{dq}_R \otimes \mathbf{dq}_R^{-1} = \mathbf{I}_q$ leads to

$$\mathbf{d}\dot{\mathbf{q}}_R^{-1} = -\mathbf{dq}_R^{-1} \otimes \mathbf{d}\dot{\mathbf{q}}_R \otimes \mathbf{dq}_R^{-1} \tag{44}$$

Using this equation in Eq. (40a) leads to

$$\mathbf{d}\dot{\mathbf{q}}_B^{-1} = -\mathbf{dq}_B^{-1} \otimes \mathbf{d}\dot{\mathbf{q}}_B \otimes \mathbf{dq}_B^{-1} \tag{45}$$

which shows that $\mathbf{dq}_B \otimes \mathbf{dq}_B^{-1} = \mathbf{I}_q$, since Eq. (45) can be derived from taken the time derivative of $\mathbf{dq}_B \otimes \mathbf{dq}_B^{-1} = \mathbf{I}_q$. This again shows that the four frames are not independent of each other.

Reference [15] states that every realization of the geometrically defined error must be expressed with respect to the same coordinate basis. Therefore, in order to express the body-frame frame errors when errors exist in both the body and reference frames it is argued here that $\mathbf{dq}_B$ is the quaternion that maps the mean body-frame vectors to the true body-frame vectors *given* the reference frame. The same analogy holds for $\mathbf{dq}_R$. The errors are now defined using a conditional probability, given by

$$\mathbf{dq}_B \triangleq E\{\mathbf{q}_{BR} \otimes \mathbf{q}_{R\hat{R}} \otimes \mathbf{q}_{\hat{R}\hat{B}} \,|\, \hat{R}\} = \mathbf{q} \otimes \hat{\mathbf{q}}^{-1} \tag{46a}$$

$$\mathbf{dq}_R \triangleq E\{\mathbf{q}_{\hat{R}\hat{B}} \otimes \mathbf{q}_{\hat{B}B} \otimes \mathbf{q}_{BR} \,|\, \hat{B}\} = \hat{\mathbf{q}}^{-1} \otimes \mathbf{q} \tag{46b}$$

Since the mean reference frame is given in the definition of Eq. (46a) then it is not treated as a random variable from a conditional point-of-view, which resolves the frame independence issue. Note that $\hat{B}$ and $\hat{R}$ are still random variables. The conditional probability definition is required to ensure that the errors in the body and reference frames have physical meaning.

Now that the body and reference error frame definitions have been established, the relationships between them are derived. Suppose that representations of some true vector are given in the body frame, denoted by $\boldsymbol{\beta}_B$, and in the reference frame, denoted by $\boldsymbol{\beta}_R$. The mapping between these two vectors is given by the attitude matrix $A(\mathbf{q})$ with

$$\boldsymbol{\beta}_B = A(\mathbf{q})\boldsymbol{\beta}_R \tag{47}$$

The attitude matrix equivalent of Eq. (46a) for the body-frame error definition is given by

$$A_B(\mathbf{dq}) = A(\mathbf{q})A^T(\hat{\mathbf{q}}) \tag{48}$$

Solving Eq. (48) for $A(\mathbf{q})$, and substituting the resultant into Eq. (47) gives

$$\boldsymbol{\beta}_B = A_B(\mathbf{dq})A(\hat{\mathbf{q}})\boldsymbol{\beta}_R \tag{49}$$

The conditional body-frame estimate, i.e. given the mean reference frame, for $\boldsymbol{\beta}_B$ is given by

$$\hat{\boldsymbol{\beta}}_B \triangleq E\{\boldsymbol{\beta}_B|\hat{R}\} = A(\hat{\mathbf{q}})\boldsymbol{\beta}_R \tag{50}$$

Using Eq. (50) in Eq. (49) gives

$$\boldsymbol{\beta}_B = A_B(\mathbf{dq})\hat{\boldsymbol{\beta}}_B \tag{51}$$

These equations are consistent with previously defined body-frame error:

$$\mathbf{d}\boldsymbol{\beta}_B \triangleq A_B^T(\mathbf{dq})\boldsymbol{\beta}_B - \hat{\boldsymbol{\beta}}_B \tag{52}$$

Substituting Eq. (49) and using Eq. (50), or substituting Eq. (50) and using Eq. (49), in Eq. (52) both give $\mathbf{d}\boldsymbol{\beta}_B = \mathbf{0}$. This analysis shows why Eq. (46a) is called the "body-referenced" error in Ref. [10], although it is not explicitly shown there. It is derived here explicitly to show the consistency of the geometrically defined body-error representation. The "unframed" error definition in Ref. [10] is not consistent with the geometrically defined body-error representation though. This unframed body-error definition is given by

$$\boldsymbol{\delta\beta}_B \triangleq \boldsymbol{\beta}_B - \hat{\boldsymbol{\beta}}_B \tag{53}$$

which is the same error definition used in all filter implementations, dating back to the earliest days of attitude estimation and inertial navigation, before the geometrically consistent filter in Ref. [15] was derived. Substituting Eq. (51) into Eq. (53) shows that $\boldsymbol{\delta\beta}_B$ clearly does not achieve the goal of having errors represented in common frames.

The attitude matrix equivalent of Eq. (46b) for the reference-frame error definition is given by

$$A_R(\mathbf{dq}) = A^T(\hat{\mathbf{q}})A(\mathbf{q}) \tag{54}$$

which is consistent with the definition given in Ref. [20]. Solving this equation for $A^T(\mathbf{q})$, and substituting it into $\boldsymbol{\beta}_R = A^T(\mathbf{q})\boldsymbol{\beta}_B$ gives

$$\boldsymbol{\beta}_R = A_R^T(\mathbf{dq})A^T(\hat{\mathbf{q}})\boldsymbol{\beta}_B \tag{55}$$

The conditional reference-frame estimate, i.e. given the mean body frame, for $\boldsymbol{\beta}_R$ is given by

$$\hat{\boldsymbol{\beta}}_R \triangleq E\{\boldsymbol{\beta}_R|\hat{B}\} = A^T(\hat{\mathbf{q}})\boldsymbol{\beta}_B \tag{56}$$

Solving Eq. (55) for $\boldsymbol{\beta}_B$, and substituting the resultant into Eq. (56) gives

$$\hat{\boldsymbol{\beta}}_R = A_R(\mathbf{dq})\boldsymbol{\beta}_R \tag{57}$$

Equations (51) and (57) have a similar form but use two different attitude-error representations. Also, note that $A_R(\mathbf{dq}) \neq A_B^T(\mathbf{dq})$. Whereas $A_B(\mathbf{dq})$ maps mean-frame body quantities to their respective true body frames, $A_R(\mathbf{dq})$ maps true-frame reference quantities to their respective mean reference frames. This is consistent with the following reference-frame error definition:

$$\mathbf{d}\boldsymbol{\beta}_R \triangleq A_R(\mathbf{dq})\boldsymbol{\beta}_R - \hat{\boldsymbol{\beta}}_R \tag{58}$$

Substituting Eq. (57) into Eq. (58) gives $\mathbf{d}\boldsymbol{\beta}_R = \mathbf{0}$, which is the desired result. As with the unframed body-error representation, the unframed reference-error representation, defined by

$$\boldsymbol{\delta}\boldsymbol{\beta}_R \triangleq \boldsymbol{\beta}_R - \hat{\boldsymbol{\beta}}_R \tag{59}$$

does not yield a frame consistent representation, which is commonly employed in INS filter applications.

The body-frame error-kinematics follow [15]

$$\dot{A}_B(\mathbf{dq}) = -A_B(\mathbf{dq})[\mathbf{d}\boldsymbol{\omega}_B\times] \tag{60}$$

where

$$\mathbf{d}\boldsymbol{\omega}_B \triangleq A_B^T(\mathbf{dq})\boldsymbol{\omega}_B - \hat{\boldsymbol{\omega}}_B \tag{61}$$

It is explicitly stated here that the true and estimated angular velocities are expressed in body-frame coordinates by the subscript B. Note that Eq. (61) shows a mapping of the body-frame angular velocities into a common frame, which is the mean frame in this case. This is akin to what is commonly seen in attitude control designs, where the desired angular velocity and actual angular velocity are also mapped into a common frame [21]. The reference-frame error-kinematics can be shown to be given by

$$\dot{A}_R(\mathbf{dq}) = -[\mathbf{d}\boldsymbol{\omega}_R\times]A_R(\mathbf{dq}) \tag{62}$$

where

$$\mathbf{d}\boldsymbol{\omega}_R \triangleq A^T(\hat{\mathbf{q}})(\boldsymbol{\omega}_B - \hat{\boldsymbol{\omega}}_B) \tag{63}$$

Note that a straight difference of $\boldsymbol{\omega}_B$ and $\hat{\boldsymbol{\omega}}_B$ now appears. This seems unnatural in the context of common frame error representations discussed in this paper. But this "unframed" difference actually comes about from the reference-frame error definition given by Eq. (46b), in which the mean body-frame is assumed to be given. By this conditional expectation any reference-frame error definition involving body-frame vectors does not require that the body-frame vectors be mapped into a common frame. Thus the unframed angular velocity in Eq. (63) is perfectly reasonable under this definition.

It is important to note that any reference-frame vector would still be mapped into a common frame under Eq. (46b) though. The respective true and estimated reference-frame angular velocities are given by

$$\boldsymbol{\omega}_R = A^T(\mathbf{q})\boldsymbol{\omega}_B \tag{64a}$$

$$\hat{\boldsymbol{\omega}}_R = A^T(\hat{\mathbf{q}})\hat{\boldsymbol{\omega}}_B \tag{64b}$$

They are also referred to as the "space-referenced angular velocity" in Ref. [5]. Solving Eq. (64) for $\boldsymbol{\omega}_B$ and $\hat{\boldsymbol{\omega}}_B$, and substituting their resultants into Eq. (63) gives

$$\mathbf{d}\boldsymbol{\omega}_R = A_R(\mathbf{dq})\boldsymbol{\omega}_R - \hat{\boldsymbol{\omega}}_R \tag{65}$$

where Eq. (54) has been used. It is now seen that the reference-frame angular velocities are mapped into a common frame.

The same analogy can be shown when reference-frame vectors are used in the body-frame error-kinematics. Solving Eq. (64) for $\boldsymbol{\omega}_B$ and $\hat{\boldsymbol{\omega}}_B$, and substituting their resultants into Eq. (61) gives

$$\mathbf{d}\boldsymbol{\omega}_B = A^T(\hat{\mathbf{q}})(\boldsymbol{\omega}_R - \hat{\boldsymbol{\omega}}_R) \tag{66}$$

where Eq. (48) has also been used. It is seen here that a straight difference of the reference-frame angular velocities is now given, which is a result of the body-frame error definition given by conditional expectation in Eq. (46b).

In INS applications errors will be defined both in the body and reference frames. For example, body-frame gyro biases and reference-frame velocity vectors are employed in an INS filter. At first, it would seem that the filter design would require both Eqs. (60) and (62) to fully describe the error-kinematics for both frames. But this is not required because $A_B(\mathbf{dq})$ is related to $A_R(\mathbf{dq})$ through

$$A_R(\mathbf{dq}) = A^T(\hat{\mathbf{q}})A_B(\mathbf{dq})A(\hat{\mathbf{q}}) \tag{67}$$

Thus, error-kinematics for either $A_B(\mathbf{dq})$ or $A_R(\mathbf{dq})$ can be used, and then Eq. (67) can be employed to map between frames. Here, the body-frame error-kinematics in Eq. (60) will be employed from this point forward, and any reference-frame errors will be mapped by Eq. (67) so that only $A_B(\mathbf{dq})$ needs to be employed for both error definitions. Hence, the GEKF in Table 1 can still be directly employed even when reference-frame errors are present. From this point forward it will be evident when body-frame vectors and reference-frame vectors are used, so the subscripts B and R will be dropped to simplify the notation.

VI. Inertial Navigation Filter Applications

This section provides applications of the GEKF for INS applications using the ECEF frame and NED frame [22]. Derivations for the GEKF are shown using both the linearization approach shown in the appendix of Ref. [15], as well as Eq. (27). Both approaches are identical for the specific models in this section, but Eq. (27) is more general.

A. ECEF Formulation

In this section the implementation equations for the EKF and GEKF using the ECEF formulation are shown. Here the quaternion maps from quantities from the E frame to the B frame. The truth equations are given by

$$\dot{\mathbf{q}} = \frac{1}{2}\Xi(\mathbf{q})\boldsymbol{\omega}^B_{B/E} \tag{68a}$$

$$\boldsymbol{\omega}^B_{B/E} = (I_{3\times3} - \mathcal{K}_g)(\tilde{\boldsymbol{\omega}}^B_{B/I} - \boldsymbol{\beta}_g - \boldsymbol{\eta}_{gv}) - A^B_E(\mathbf{q})\boldsymbol{\omega}^E_{E/I} \tag{68b}$$

$$\dot{\mathbf{v}}^E = -[\boldsymbol{\omega}^E_{E/I}\times][\boldsymbol{\omega}^E_{E/I}\times]\mathbf{p}^E - 2[\boldsymbol{\omega}^E_{E/I}\times]\mathbf{v}^E + A^E_B(\mathbf{q})\mathbf{a}^B + \mathbf{g}^E \tag{68c}$$

$$\mathbf{a}^B = (I_{3\times3} - \mathcal{K}_a)(\tilde{\mathbf{a}}^B - \boldsymbol{\beta}_a - \boldsymbol{\eta}_{av}) \tag{68d}$$

$$\mathbf{g}^E = \frac{-\mu}{||\mathbf{p}^E||^3}\mathbf{p}^E \tag{68e}$$

$$\dot{\boldsymbol{\beta}}_g = \boldsymbol{\eta}_{gu} \tag{68f}$$

$$\dot{\boldsymbol{\beta}}_a = \boldsymbol{\eta}_{au} \tag{68g}$$

$$\dot{\mathbf{k}}_g = \mathbf{0} \tag{68h}$$

$$\dot{\mathbf{k}}_a = \mathbf{0} \tag{68i}$$

where $\mathbf{k}_g$ and $\mathbf{k}_a$ are the elements of the diagonal matrices $\mathcal{K}_g$ and $\mathcal{K}_a$, respectively. Also, where $\boldsymbol{\omega}^E_{E/I}$ is the angular velocity of the E frame relative to the I frame expressed in E coordinates. The angular velocity

vector is simply given by $\boldsymbol{\omega}^E_{E/I} = [0\ \ 0\ \ \omega_e]^T$, where ω_e is the Earth's rotation rate given as (from WGS-84) 7.292115×10^{-5} rad/sec. The gravity model is given by

$$\mathbf{g}^E = \frac{-\mu}{||\mathbf{p}^E||^3}\mathbf{p}^E \tag{69}$$

where $\mu = 3.986004415\ \text{km}^3/\text{sec}^2$.

The estimated quantities are given by

$$\dot{\hat{\mathbf{q}}} = \frac{1}{2}\Xi(\hat{\mathbf{q}})\hat{\boldsymbol{\omega}}^B_{B/E} \tag{70a}$$

$$\hat{\boldsymbol{\omega}}^B_{B/E} = (I_{3\times3} - \hat{\mathcal{K}}_g)(\tilde{\boldsymbol{\omega}}^B_{B/I} - \hat{\boldsymbol{\beta}}_g) - A^B_E(\hat{\mathbf{q}})\boldsymbol{\omega}^E_{E/I} \tag{70b}$$

$$\dot{\hat{\mathbf{v}}}^E = -[\boldsymbol{\omega}^E_{E/I}\times][\boldsymbol{\omega}^E_{E/I}\times]\hat{\mathbf{p}}^E - 2[\boldsymbol{\omega}^E_{E/I}\times]\hat{\mathbf{v}}^E + A^E_B(\hat{\mathbf{q}})\hat{\mathbf{a}}^B + \hat{\mathbf{g}}^E \tag{70c}$$

$$\hat{\mathbf{a}}^B = (I_{3\times3} - \hat{\mathcal{K}}_a)(\tilde{\mathbf{a}}^B - \hat{\boldsymbol{\beta}}_a) \tag{70d}$$

$$\hat{\mathbf{g}}^E = \frac{-\mu}{||\hat{\mathbf{p}}^E||^3}\hat{\mathbf{p}}^E \tag{70e}$$

$$\dot{\hat{\boldsymbol{\beta}}}_g = \mathbf{0} \tag{70f}$$

$$\dot{\hat{\boldsymbol{\beta}}}_a = \mathbf{0} \tag{70g}$$

$$\dot{\hat{\mathbf{k}}}_g = \mathbf{0} \tag{70h}$$

$$\dot{\hat{\mathbf{k}}}_a = \mathbf{0} \tag{70i}$$

Note that the attitude matrix is coupled into the position, which allows estimation of the attitude from position measurements.

1. *Extended Kalman Filter Formulation*

The global state vector, local state-error vector, process noise vector and spectral density used in the EKF are defined as

$$\mathbf{x} \triangleq \begin{bmatrix} \mathbf{q} \\ \mathbf{p}^E \\ \mathbf{v}^E \\ \boldsymbol{\beta}_g \\ \boldsymbol{\beta}_a \\ \mathbf{k}_g \\ \mathbf{k}_a \end{bmatrix}, \quad \Delta\mathbf{x} \triangleq \begin{bmatrix} \boldsymbol{\delta\alpha} \\ \Delta\mathbf{p}^E \\ \Delta\mathbf{v}^E \\ \Delta\boldsymbol{\beta}_g \\ \Delta\boldsymbol{\beta}_a \\ \Delta\mathbf{k}_g \\ \Delta\mathbf{k}_a \end{bmatrix}, \quad \mathbf{w} \triangleq \begin{bmatrix} \boldsymbol{\eta}_{gv} \\ \boldsymbol{\eta}_{gu} \\ \boldsymbol{\eta}_{av} \\ \boldsymbol{\eta}_{au} \end{bmatrix} \tag{71a}$$

$$Q = \begin{bmatrix} \sigma^2_{gv}I_{3\times3} & 0_{3\times3} & 0_{3\times3} & 0_{3\times3} \\ 0_{3\times3} & \sigma^2_{gu}I_{3\times3} & 0_{3\times3} & 0_{3\times3} \\ 0_{3\times3} & 0_{3\times3} & \sigma^2_{av}I_{3\times3} & 0_{3\times3} \\ 0_{3\times3} & 0_{3\times3} & 0_{3\times3} & \sigma^2_{au}I_{3\times3} \end{bmatrix} \tag{71b}$$

Note that the notation $\boldsymbol{\delta\alpha}$ is used here for the attitude error-vector to specifically differentiate it from the geometric filter definition. The error-dynamics used in the EKF propagation are given by

$$\Delta\dot{\mathbf{x}} = F\Delta\mathbf{x} + G\mathbf{w} \tag{72}$$

where

$$F = \begin{bmatrix} F_{11} & 0_{3\times3} & 0_{3\times3} & F_{14} & 0_{3\times3} & F_{16} & 0_{3\times3} \\ 0_{3\times3} & 0_{3\times3} & I_{3\times3} & 0_{3\times3} & 0_{3\times3} & 0_{3\times3} & 0_{3\times3} \\ F_{31} & F_{32} & F_{33} & 0_{3\times3} & F_{35} & 0_{3\times3} & F_{37} \\ 0_{3\times3} & 0_{3\times3} & 0_{3\times3} & 0_{3\times3} & 0_{3\times3} & 0_{3\times3} & 0_{3\times3} \\ 0_{3\times3} & 0_{3\times3} & 0_{3\times3} & 0_{3\times3} & 0_{3\times3} & 0_{3\times3} & 0_{3\times3} \\ 0_{3\times3} & 0_{3\times3} & 0_{3\times3} & 0_{3\times3} & 0_{3\times3} & 0_{3\times3} & 0_{3\times3} \\ 0_{3\times3} & 0_{3\times3} & 0_{3\times3} & 0_{3\times3} & 0_{3\times3} & 0_{3\times3} & 0_{3\times3} \end{bmatrix} \tag{73a}$$

$$G = \begin{bmatrix} -(I_{3\times3} - \hat{\mathcal{K}}_g) & 0_{3\times3} & 0_{3\times3} & 0_{3\times3} \\ 0_{3\times3} & 0_{3\times3} & 0_{3\times3} & 0_{3\times3} \\ 0_{3\times3} & 0_{3\times3} & -A_B^E(\hat{\mathbf{q}})(I_{3\times3} - \hat{\mathcal{K}}_a) & 0_{3\times3} \\ 0_{3\times3} & I_{3\times3} & 0_{3\times3} & 0_{3\times3} \\ 0_{3\times3} & 0_{3\times3} & 0_{3\times3} & I_{3\times3} \\ 0_{3\times3} & 0_{3\times3} & 0_{3\times3} & 0_{3\times3} \\ 0_{3\times3} & 0_{3\times3} & 0_{3\times3} & 0_{3\times3} \end{bmatrix} \tag{73b}$$

with

$$F_{11} = -\left[\left(\hat{\boldsymbol{\omega}}_{B/E}^B + A_E^B(\hat{\mathbf{q}})\boldsymbol{\omega}_{E/I}^E\right)\times\right] \tag{74a}$$

$$F_{14} = -(I_{3\times3} - \hat{\mathcal{K}}_g) \tag{74b}$$

$$F_{16} = -\mathbb{D}(\tilde{\boldsymbol{\omega}}_{B/I}^B - \hat{\boldsymbol{\beta}}_g) \tag{74c}$$

$$F_{31} = -A_B^E(\hat{\mathbf{q}})[\hat{\mathbf{a}}^B\times] \tag{74d}$$

$$F_{32} = U(\hat{\mathbf{p}}^E) - [\boldsymbol{\omega}_{E/I}^E\times][\boldsymbol{\omega}_{E/I}^E\times] \tag{74e}$$

$$F_{33} = -2[\boldsymbol{\omega}_{E/I}^E\times] \tag{74f}$$

$$F_{35} = -A_B^E(\hat{\mathbf{q}})(I_{3\times3} - \hat{\mathcal{K}}_a) \tag{74g}$$

$$F_{37} = -A_B^E(\hat{\mathbf{q}})\mathbb{D}(\tilde{\mathbf{a}}^B - \hat{\boldsymbol{\beta}}_a) \tag{74h}$$

where $\mathbb{D}(\mathbf{z})$ denotes a diagonal matrix made up of the elements of any vector $\mathbf{z}$, and

$$U(\hat{\mathbf{p}}^E) \triangleq -\mu\left(I_{3\times3}\left|\left|\hat{\mathbf{p}}^E\right|\right|^{-3} - 3(\hat{\mathbf{p}}^E)(\hat{\mathbf{p}}^E)^T\left|\left|\hat{\mathbf{p}}^E\right|\right|^{-5}\right) \tag{75}$$

which is the gravity gradient expression. The standard EKF can now be applied using the expressions in this section.

2. Geometric Extended Kalman Filter Formulation

The global state and local state-error vectors in the GEKF are defined as

$$\mathbf{x} \triangleq \begin{bmatrix} \mathbf{q} \\ \mathbf{p}^E \\ \mathbf{v}^E \\ \boldsymbol{\beta}_g \\ \boldsymbol{\beta}_a \\ \mathbf{k}_g \\ \mathbf{k}_a \end{bmatrix}, \quad \mathbf{dx} \triangleq \begin{bmatrix} \mathbf{d}\boldsymbol{\alpha} \\ \mathbf{dp}^E \\ \mathbf{dv}^E \\ \mathbf{d}\boldsymbol{\beta}_g \\ \mathbf{d}\boldsymbol{\beta}_a \\ \mathbf{dk}_g \\ \mathbf{dk}_a \end{bmatrix} \tag{76}$$

The quaternion error follows from Eq. (19a), and the bias and scale factor errors for the gyro and accelerometer follow from Eq. (19b). The position error needs to be discussed. The dynamics now occur at the acceleration level. The geometric position error is equivalent to the standard difference error because the

derivative of position is velocity, which is a pure kinematic relationship, independent of the frame. Thus the geometric position error is given by

$$\mathbf{dp}^E = \mathbf{p}^E - \hat{\mathbf{p}}^E \tag{77}$$

From the previous developments, i.e. with the use of Eq. (67), the geometric velocity-error is given by

$$\mathbf{dv}^E = A_B^E(\hat{\mathbf{q}})A(\mathbf{dq})A_E^B(\hat{\mathbf{q}})\mathbf{v}^E - \hat{\mathbf{v}}^E \tag{78}$$

where $A(\mathbf{dq})$ is equivalent to $A_B(\mathbf{dq})$. Substituting Eq. (18) into Eq. (78) gives

$$\begin{aligned}\mathbf{dv}^E &= \mathbf{v}^E - \hat{\mathbf{v}}^E - A_B^E(\hat{\mathbf{q}})[\mathbf{d}\boldsymbol{\alpha}\times]A_E^B(\hat{\mathbf{q}})\mathbf{v}^E \\ &= \mathbf{v}^E - \hat{\mathbf{v}}^E + A_B^E(\hat{\mathbf{q}})[A_E^B(\hat{\mathbf{q}})\mathbf{v}^E\times]\mathbf{d}\boldsymbol{\alpha} \\ &= \mathbf{v}^E - \hat{\mathbf{v}}^E + [\mathbf{v}^E\times]A_B^E(\hat{\mathbf{q}})\mathbf{d}\boldsymbol{\alpha}\end{aligned} \tag{79}$$

where the identity $[A_E^B(\hat{\mathbf{q}})\mathbf{v}^E\times] = A_E^B(\hat{\mathbf{q}})[\mathbf{v}^E\times]A_B^E(\hat{\mathbf{q}})$ has been used. Then the matrices C and $\dot{C}$ are given by

$$C = \begin{bmatrix} \frac{1}{2}\Xi(\hat{\mathbf{q}}) & 0_{4\times3} & 0_{4\times3} & 0_{4\times3} & 0_{4\times3} & 0_{4\times3} & 0_{4\times3} \\ 0_{3\times3} & I_{3\times3} & 0_{3\times3} & 0_{3\times3} & 0_{3\times3} & 0_{3\times3} & 0_{3\times3} \\ -[\hat{\mathbf{v}}^E\times]A_B^E(\hat{\mathbf{q}}) & 0_{3\times3} & I_{3\times3} & 0_{3\times3} & 0_{3\times3} & 0_{3\times3} & 0_{3\times3} \\ [\hat{\boldsymbol{\beta}}_g\times] & 0_{3\times3} & 0_{3\times3} & I_{3\times3} & 0_{3\times3} & 0_{3\times3} & 0_{3\times3} \\ [\hat{\boldsymbol{\beta}}_a\times] & 0_{3\times3} & 0_{3\times3} & 0_{3\times3} & I_{3\times3} & 0_{3\times3} & 0_{3\times3} \\ [\hat{\mathbf{k}}_g\times] & 0_{3\times3} & 0_{3\times3} & 0_{3\times3} & 0_{3\times3} & I_{3\times3} & 0_{3\times3} \\ [\hat{\mathbf{k}}_a\times] & 0_{3\times3} & 0_{3\times3} & 0_{3\times3} & 0_{3\times3} & 0_{3\times3} & I_{3\times3} \end{bmatrix} \tag{80a}$$

$$\dot{C} = \begin{bmatrix} \frac{1}{4}\Omega(\hat{\boldsymbol{\omega}}_{B/E}^B)\Xi(\hat{\mathbf{q}}) + \frac{1}{2}\Xi(\hat{\mathbf{q}})[\hat{\boldsymbol{\omega}}_{B/E}^B\times] & 0_{4\times3} & 0_{4\times3} & 0_{4\times3} & 0_{4\times3} & 0_{4\times3} & 0_{4\times3} \\ 0_{3\times3} & 0_{3\times3} & 0_{3\times3} & 0_{3\times3} & 0_{3\times3} & 0_{3\times3} & 0_{3\times3} \\ -[\dot{\hat{\mathbf{v}}}^E\times]A_B^E(\hat{\mathbf{q}}) - [\hat{\mathbf{v}}^E\times]A_B^E(\hat{\mathbf{q}})[\hat{\boldsymbol{\omega}}_{B/E}^B\times] & 0_{3\times3} & 0_{3\times3} & 0_{3\times3} & 0_{3\times3} & 0_{3\times3} & 0_{3\times3} \\ 0_{3\times3} & 0_{3\times3} & 0_{3\times3} & 0_{3\times3} & 0_{3\times3} & 0_{3\times3} & 0_{3\times3} \\ 0_{3\times3} & 0_{3\times3} & 0_{3\times3} & 0_{3\times3} & 0_{3\times3} & 0_{3\times3} & 0_{3\times3} \\ 0_{3\times3} & 0_{3\times3} & 0_{3\times3} & 0_{3\times3} & 0_{3\times3} & 0_{3\times3} & 0_{3\times3} \\ 0_{3\times3} & 0_{3\times3} & 0_{3\times3} & 0_{3\times3} & 0_{3\times3} & 0_{3\times3} & 0_{3\times3} \end{bmatrix} \tag{80b}$$

where the time derivative of $\Xi(\hat{\mathbf{q}})$ is given in Appendix A of Ref. [5]. These matrices can now be used directly in the GEKF equations.

The matrices F_a and G_a need to be derived. In order to do this, the partial $\|\mathbf{q}\|^{-2}A^T(\mathbf{q})\mathbf{u}$ with respect to $\mathbf{q}$ will be needed, where $A(\mathbf{q})$ is any attitude matrix parameterized using the quaternion and $\mathbf{u}$ is any general 3×1 vector. This procedure follows along the lines given in Appendix A of Ref. [5], which proves

$$\frac{\partial}{\partial\mathbf{q}}\left[A(\mathbf{q})\mathbf{u}\right] = 2\|\mathbf{q}\|^{-2}[A(\mathbf{q})\mathbf{u}\times]\Xi^T(\mathbf{q}) \tag{81}$$

The attitude matrix is given by Eq. (5). Using the identity $\Xi(\mathbf{q})\mathbf{u} = \Omega(\mathbf{u})\mathbf{q}$ leads to

$$Z \triangleq \frac{\partial}{\partial\mathbf{q}}\left[\|\mathbf{q}\|^{-2}A^T(\mathbf{q})\mathbf{u}\right] = \frac{\partial}{\partial\mathbf{q}}\left[\|\mathbf{q}\|^{-2}\Psi^T(\mathbf{q})\bar{\mathbf{q}}\right] \tag{82}$$

where $\bar{\mathbf{q}} \triangleq \Omega(\mathbf{u})\mathbf{q}$. This leads to

$$Z = \|\mathbf{q}\|^{-2}\left[\frac{\partial}{\partial\mathbf{q}}\Psi^T(\mathbf{q})\bar{\mathbf{q}}\right] + \|\mathbf{q}\|^{-2}\Psi^T(\mathbf{q})\Omega(\mathbf{u}) - 2\|\mathbf{q}\|^{-4}\Psi^T(\mathbf{q})\Omega(\mathbf{u})\mathbf{q}\,\mathbf{q}^T \tag{83}$$

Using the identities $\Psi^T(\mathbf{q})\bar{\mathbf{q}} = -\Psi^T(\bar{\mathbf{q}})\mathbf{q}$ and $\Psi^T(\bar{\mathbf{q}}) = -\Psi^T(\mathbf{q})\Omega(\mathbf{u})$, which is Eq. (A.39f) in Ref. [5], leads to

$$\begin{aligned}Z &= \|\mathbf{q}\|^{-2}\Psi^T(\mathbf{q})\Omega(\mathbf{u}) + \|\mathbf{q}\|^{-2}\Psi^T(\mathbf{q})\Omega(\mathbf{u}) - 2\|\mathbf{q}\|^{-4}\Psi^T(\mathbf{q})\Omega(\mathbf{u})\mathbf{q}\,\mathbf{q}^T \\ &= 2\|\mathbf{q}\|^{-2}\Psi^T(\mathbf{q})\Omega(\mathbf{u}) - 2\|\mathbf{q}\|^{-4}\Psi^T(\mathbf{q})\Omega(\mathbf{u})\mathbf{q}\,\mathbf{q}^T \\ &= 2\|\mathbf{q}\|^{-4}\Psi^T(\mathbf{q})\Omega(\mathbf{u})\left(\|\mathbf{q}\|^2 I_{4\times4} - \mathbf{q}\,\mathbf{q}^T\right)\end{aligned} \tag{84}$$

Next, using the identity $\Psi(\mathbf{q})\Psi^T(\mathbf{q}) = \|\mathbf{q}\|^2 I_{4\times4} - \mathbf{q}\,\mathbf{q}^T$ gives

$$Z = 2\|\mathbf{q}\|^{-4}\Psi^T(\mathbf{q})\Omega(\mathbf{u})\Psi(\mathbf{q})\Psi^T(\mathbf{q}) \tag{85}$$

Finally, using the identity $\Psi^T(\mathbf{q})\Omega(\mathbf{u})\Psi(\mathbf{q}) = -\|\mathbf{q}\|^{-2}[A^T(\mathbf{q})\mathbf{u}\times]$, which is Eq. (A.39d) in Ref. [5], gives the desired result:

$$Z = -2\|\mathbf{q}\|^{-2}[A^T(\mathbf{q})\mathbf{u}\times]\Psi^T(\mathbf{q}) \tag{86}$$

where $\|\mathbf{q}\| = 1$ can now be assumed. Therefore, the matrix F_a is given by

$$F_a = \begin{bmatrix} F_{a_{11}} & 0_{4\times3} & 0_{4\times3} & F_{a_{14}} & 0_{4\times3} & F_{a_{16}} & 0_{4\times3} \\ 0_{3\times4} & 0_{3\times3} & I_{3\times3} & 0_{3\times3} & 0_{3\times3} & 0_{3\times3} & 0_{3\times3} \\ F_{a_{31}} & F_{a_{32}} & F_{a_{33}} & 0_{3\times3} & F_{a_{35}} & 0_{3\times3} & F_{a_{37}} \\ 0_{3\times4} & 0_{3\times3} & 0_{3\times3} & 0_{3\times3} & 0_{3\times3} & 0_{3\times3} & 0_{3\times3} \\ 0_{3\times4} & 0_{3\times3} & 0_{3\times3} & 0_{3\times3} & 0_{3\times3} & 0_{3\times3} & 0_{3\times3} \\ 0_{3\times4} & 0_{3\times3} & 0_{3\times3} & 0_{3\times3} & 0_{3\times3} & 0_{3\times3} & 0_{3\times3} \\ 0_{3\times4} & 0_{3\times3} & 0_{3\times3} & 0_{3\times3} & 0_{3\times3} & 0_{3\times3} & 0_{3\times3} \end{bmatrix} \tag{87}$$

with

$$F_{a_{11}} = \frac{1}{2}\Omega(\hat{\boldsymbol{\omega}}^B_{B/E}) - \Xi(\hat{\mathbf{q}})\left[A^B_E(\hat{\mathbf{q}})\boldsymbol{\omega}^E_{E/I}\times\right]\Xi^T(\hat{\mathbf{q}}) \tag{88a}$$

$$F_{a_{14}} = -\frac{1}{2}\Xi(\hat{\mathbf{q}})(I_{3\times3} - \hat{\mathcal{K}}_g) \tag{88b}$$

$$F_{a_{16}} = -\frac{1}{2}\Xi(\hat{\mathbf{q}})\mathbb{D}(\tilde{\boldsymbol{\omega}}^B_{B/I} - \hat{\boldsymbol{\beta}}_g) \tag{88c}$$

$$F_{a_{31}} = -2[A^E_B(\hat{\mathbf{q}})\hat{\mathbf{a}}^B\times]\Psi^T(\hat{\mathbf{q}}) \tag{88d}$$

$$F_{a_{32}} = U(\hat{\mathbf{p}}^E) - [\boldsymbol{\omega}^E_{E/I}\times][\boldsymbol{\omega}^E_{E/I}\times] \tag{88e}$$

$$F_{a_{33}} = -2[\boldsymbol{\omega}^E_{E/I}\times] \tag{88f}$$

$$F_{a_{35}} = -A^E_B(\hat{\mathbf{q}})(I_{3\times3} - \hat{\mathcal{K}}_a) \tag{88g}$$

$$F_{a_{37}} = -A^E_B(\hat{\mathbf{q}})\mathbb{D}(\tilde{\mathbf{a}}^B - \hat{\boldsymbol{\beta}}_a) \tag{88h}$$

The matrix G_a is given by

$$G_a = \begin{bmatrix} -\frac{1}{2}\Xi(\hat{\mathbf{q}})(I_{3\times3} - \hat{\mathcal{K}}_g) & 0_{4\times3} & 0_{4\times3} & 0_{4\times3} \\ 0_{3\times3} & 0_{3\times3} & 0_{3\times3} & 0_{3\times3} \\ 0_{3\times3} & 0_{3\times3} & -A^E_B(\hat{\mathbf{q}})(I_{3\times3} - \hat{\mathcal{K}}_a) & 0_{3\times3} \\ 0_{3\times3} & I_{3\times3} & 0_{3\times3} & 0_{3\times3} \\ 0_{3\times3} & 0_{3\times3} & 0_{3\times3} & I_{3\times3} \\ 0_{3\times3} & 0_{3\times3} & 0_{3\times3} & 0_{3\times3} \\ 0_{3\times3} & 0_{3\times3} & 0_{3\times3} & 0_{3\times3} \end{bmatrix} \tag{89}$$

The matrices F_g and G_g can now be derived using Eq. (27).

B. NED Formulation

In this section the implementation equations for the EKF and GEKF using the NED formulation are shown. Here the quaternion maps quantities from the N frame to the B frame. The truth equations are given by

$$\dot{\mathbf{q}} = \frac{1}{2}\Xi(\mathbf{q})\boldsymbol{\omega}^B_{B/N} \tag{90a}$$

$$\dot{\phi} = \frac{v_N}{R_\phi + h} \tag{90b}$$

$$\dot{\lambda} = \frac{v_E}{(R_\lambda + h)\cos\phi} \tag{90c}$$

$$\dot{h} = -v_D \tag{90d}$$

$$\dot{v}_N = -\left[\frac{v_E}{(R_\lambda + h)\cos\phi} + 2\omega_e\right] v_E \sin\phi + \frac{v_N v_D}{R_\phi + h} + a_N \tag{90e}$$

$$\dot{v}_E = \left[\frac{v_E}{(R_\lambda + h)\cos\phi} + 2\omega_e\right] v_N \sin\phi + \frac{v_E v_D}{R_\lambda + h} + 2\omega_e v_D \cos\phi + a_E \tag{90f}$$

$$\dot{v}_D = -\frac{v_E^2}{R_\lambda + h} - \frac{v_N^2}{R_\phi + h} - 2\omega_e v_E \cos\phi + g + a_D \tag{90g}$$

where $\boldsymbol{\omega}^B_{B/N}$ is the angular velocity of the B frame relative to the N frame expressed in B coordinates, and

$$R_\phi = \frac{a(1-e^2)}{(1 - e^2 \sin^2\phi)^{3/2}} \tag{91a}$$

$$R_\lambda = \frac{a}{(1 - e^2 \sin^2\phi)^{1/2}} \tag{91b}$$

The local gravity, g, using WGS-84 parameters, is given by

$$\begin{aligned} g = {} & 9.780327(1 + 5.3024 \times 10^{-3} \sin^2\phi - 5.8 \times 10^{-6} \sin^2 2\phi) \\ & - (3.0877 \times 10^{-6} - 4.4 \times 10^{-9} \sin^2\phi)h + 7.2 \times 10^{-14} h^2 \ \text{ m/sec}^2 \end{aligned} \tag{92}$$

where h is measured in meters. Note that Eq. (90a) cannot be used directly with the gyro measurement. However, this problem can be overcome by using the following identity:

$$\boldsymbol{\omega}^B_{B/I} = \boldsymbol{\omega}^B_{B/N} + \boldsymbol{\omega}^B_{N/I} \tag{93}$$

Solving Eq. (93) for $\boldsymbol{\omega}^B_{B/N}$ and substituting $\boldsymbol{\omega}^B_{N/I} = A^B_N(\mathbf{q})\boldsymbol{\omega}^N_{N/I}$ yields

$$\boldsymbol{\omega}^B_{B/N} = \boldsymbol{\omega}^B_{B/I} - A^B_N(\mathbf{q})\boldsymbol{\omega}^N_{N/I} \tag{94}$$

where

$$\boldsymbol{\omega}^N_{N/I} = \omega_e \begin{bmatrix} \cos\phi \\ 0 \\ -\sin\phi \end{bmatrix} + \begin{bmatrix} \dfrac{v_E}{R_\lambda + h} \\ -\dfrac{v_N}{R_\phi + h} \\ -\dfrac{v_E \tan\phi}{R_\lambda + h} \end{bmatrix} \tag{95}$$

Now, Eq. (90a) can be related to the gyro measurements. Also, the acceleration variables are related to the accelerometer measurements through

$$\mathbf{a}^N \triangleq \begin{bmatrix} a_N \\ a_E \\ a_D \end{bmatrix} = A^N_B(\mathbf{q})\mathbf{a}^B = A^N_B(\mathbf{q})(I_{3\times 3} - \mathcal{K}_a)(\tilde{\mathbf{a}}^B - \boldsymbol{\beta}_a - \boldsymbol{\eta}_{av}) \tag{96}$$

where $\mathbf{a}^B$ is the acceleration vector in body coordinates, and $A^N_B(\mathbf{q})$ is the matrix transpose of $A^B_N(\mathbf{q})$.

The estimated quantities, assuming ω_e is exact, are given by

$$\dot{\hat{\mathbf{q}}} = \frac{1}{2}\Xi(\hat{\mathbf{q}})\hat{\boldsymbol{\omega}}^B_{B/N} \tag{97a}$$

$$\hat{\boldsymbol{\omega}}^B_{B/N} = (I_{3\times3} - \hat{\mathcal{K}}_g)(\tilde{\boldsymbol{\omega}}^B_{B/I} - \hat{\boldsymbol{\beta}}_g) - A^B_N(\hat{\mathbf{q}})\hat{\boldsymbol{\omega}}^N_{N/I} \tag{97b}$$

$$\dot{\hat{\phi}} = \frac{\hat{v}_N}{\hat{R}_\phi + \hat{h}} \tag{97c}$$

$$\dot{\hat{\lambda}} = \frac{\hat{v}_E}{(\hat{R}_\lambda + \hat{h})\cos\hat{\phi}} \tag{97d}$$

$$\dot{\hat{h}} = -\hat{v}_D \tag{97e}$$

$$\dot{\hat{v}}_N = -\left[\frac{\hat{v}_E}{(\hat{R}_\lambda + \hat{h})\cos\hat{\phi}} + 2\omega_e\right]\hat{v}_E \sin\hat{\phi} + \frac{\hat{v}_N\hat{v}_D}{\hat{R}_\phi + \hat{h}} + \hat{a}_N \tag{97f}$$

$$\dot{\hat{v}}_E = \left[\frac{\hat{v}_E}{(\hat{R}_\lambda + \hat{h})\cos\hat{\phi}} + 2\omega_e\right]\hat{v}_N \sin\hat{\phi} + \frac{\hat{v}_E\hat{v}_D}{\hat{R}_\lambda + \hat{h}} + 2\omega_e\hat{v}_D\cos\hat{\phi} + \hat{a}_E \tag{97g}$$

$$\dot{\hat{v}}_D = -\frac{\hat{v}^2_E}{\hat{R}_\lambda + \hat{h}} - \frac{\hat{v}^2_N}{\hat{R}_\phi + \hat{h}} - 2\omega_e\hat{v}_E\cos\hat{\phi} + \hat{g} + \hat{a}_D \tag{97h}$$

$$\hat{\mathbf{a}}^N \equiv \begin{bmatrix}\hat{a}_N \\ \hat{a}_E \\ \hat{a}_D\end{bmatrix} = A^N_B(\hat{\mathbf{q}})\hat{\mathbf{a}}^B \tag{97i}$$

$$\hat{\mathbf{a}}^B = (I_{3\times3} - \hat{\mathcal{K}}_a)(\tilde{\mathbf{a}}^B - \hat{\boldsymbol{\beta}}_a) \tag{97j}$$

$$\dot{\hat{\boldsymbol{\beta}}}_g = \mathbf{0} \tag{97k}$$

$$\dot{\hat{\boldsymbol{\beta}}}_a = \mathbf{0} \tag{97l}$$

$$\dot{\hat{\mathbf{k}}}_g = \mathbf{0} \tag{97m}$$

$$\dot{\hat{\mathbf{k}}}_a = \mathbf{0} \tag{97n}$$

Also, $\hat{\boldsymbol{\omega}}^N_{N/I}$, $\hat{R}_\phi$, $\hat{R}_\lambda$, and $\hat{g}$ are evaluated at the current estimates.

The EKF formulation is shown in Ref. [19], which is not repeated here for brevity. The global state and local state-error vectors in the GEKF are defined as

$$\mathbf{x} \triangleq \begin{bmatrix}\mathbf{q} \\ \mathbf{p}^N \\ \mathbf{v}^N \\ \boldsymbol{\beta}_g \\ \boldsymbol{\beta}_a \\ \mathbf{k}_g \\ \mathbf{k}_a\end{bmatrix}, \quad \mathbf{dx} \triangleq \begin{bmatrix}\mathbf{d}\boldsymbol{\alpha} \\ \mathbf{dp}^N \\ \mathbf{dv}^N \\ \mathbf{d}\boldsymbol{\beta}_g \\ \mathbf{d}\boldsymbol{\beta}_a \\ \mathbf{dk}_g \\ \mathbf{dk}_a\end{bmatrix} \tag{98}$$

where $\mathbf{p}^N = [\phi \;\; \lambda \;\; h]^T$ and $\mathbf{v}^N = [v_N \;\; v_E \;\; v_D]^T$. The matrix F_a is given by

$$F_a = \begin{bmatrix}
F_{a_{11}} & F_{a_{12}} & F_{a_{13}} & F_{a_{14}} & 0_{4\times3} & F_{a_{16}} & 0_{4\times3} \\
0_{3\times4} & F_{a_{22}} & F_{a_{23}} & 0_{3\times3} & 0_{3\times3} & 0_{3\times3} & 0_{3\times3} \\
F_{a_{31}} & F_{a_{32}} & F_{a_{33}} & 0_{3\times3} & F_{a_{35}} & 0_{3\times3} & F_{a_{37}} \\
0_{3\times4} & 0_{3\times3} & 0_{3\times3} & 0_{3\times3} & 0_{3\times3} & 0_{3\times3} & 0_{3\times3} \\
0_{3\times4} & 0_{3\times3} & 0_{3\times3} & 0_{3\times3} & 0_{3\times3} & 0_{3\times3} & 0_{3\times3} \\
0_{3\times4} & 0_{3\times3} & 0_{3\times3} & 0_{3\times3} & 0_{3\times3} & 0_{3\times3} & 0_{3\times3} \\
0_{3\times4} & 0_{3\times3} & 0_{3\times3} & 0_{3\times3} & 0_{3\times3} & 0_{3\times3} & 0_{3\times3}
\end{bmatrix} \tag{99}$$

with

$$F_{a_{11}} = \frac{1}{2}\Omega(\hat{\boldsymbol{\omega}}^B_{B/N}) - \Xi(\hat{\mathbf{q}})\left[A^B_N(\hat{\mathbf{q}})\hat{\boldsymbol{\omega}}^N_{N/I}\times\right]\Xi^T(\hat{\mathbf{q}}) \tag{100a}$$

$$F_{a_{12}} = -\frac{1}{2}\Xi(\hat{\mathbf{q}})A^B_N(\hat{\mathbf{q}})\left.\frac{\partial\boldsymbol{\omega}^N_{N/I}}{\partial\mathbf{p}^N}\right|_{\hat{\mathbf{p}}^N,\hat{\mathbf{v}}^N}, \quad F_{a_{13}} = -\frac{1}{2}\Xi(\hat{\mathbf{q}})A^B_N(\hat{\mathbf{q}})\left.\frac{\partial\boldsymbol{\omega}^N_{N/I}}{\partial\mathbf{v}^N}\right|_{\hat{\mathbf{p}}^N,\hat{\mathbf{v}}^N} \tag{100b}$$

$$F_{a_{14}} = -\frac{1}{2}\Xi(\hat{\mathbf{q}})(I_{3\times3} - \hat{\mathcal{K}}_g), \quad F_{a_{16}} = -\frac{1}{2}\Xi(\hat{\mathbf{q}})\mathbb{D}(\tilde{\boldsymbol{\omega}}^B_{B/I} - \hat{\boldsymbol{\beta}}_g) \tag{100c}$$

$$F_{a_{22}} = \left.\frac{\partial\dot{\mathbf{p}}^N}{\partial\mathbf{p}^N}\right|_{\hat{\mathbf{p}}^N,\hat{\mathbf{v}}^N}, \quad F_{a_{23}} = \left.\frac{\partial\dot{\mathbf{p}}^N}{\partial\mathbf{v}^N}\right|_{\hat{\mathbf{p}}^N,\hat{\mathbf{v}}^N} \tag{100d}$$

$$F_{a_{31}} = -2[A^N_B(\hat{\mathbf{q}})\hat{\mathbf{a}}^B\times]\Psi^T(\hat{\mathbf{q}}) \tag{100e}$$

$$F_{a_{32}} = \left.\frac{\partial\dot{\mathbf{v}}^N}{\partial\mathbf{p}^N}\right|_{\hat{\mathbf{p}}^N,\hat{\mathbf{v}}^N}, \quad F_{a_{33}} = \left.\frac{\partial\dot{\mathbf{v}}^N}{\partial\mathbf{v}^N}\right|_{\hat{\mathbf{p}}^N,\hat{\mathbf{v}}^N} \tag{100f}$$

$$F_{a_{35}} = -A^N_B(\hat{\mathbf{q}})(I_{3\times3} - \hat{\mathcal{K}}_a), \quad F_{a_{37}} = -A^N_B(\hat{\mathbf{q}})\mathbb{D}(\tilde{\mathbf{a}}^B - \hat{\boldsymbol{\beta}}_a) \tag{100g}$$

The angular velocity partials are given by

$$\frac{\partial\boldsymbol{\omega}^N_{N/I}}{\partial\mathbf{p}^N} = \begin{bmatrix} -\omega_e\sin\phi - \dfrac{v_E}{(R_\lambda+h)^2}\dfrac{\partial R_\lambda}{\partial\phi} & 0 & -\dfrac{v_E}{(R_\lambda+h)^2} \\ \dfrac{v_N}{(R_\phi+h)^2}\dfrac{\partial R_\phi}{\partial\phi} & 0 & \dfrac{v_N}{(R_\phi+h)^2} \\ -\omega_e\cos\phi - \dfrac{v_E\sec^2\phi}{R_\lambda+h} + \dfrac{v_E\tan\phi}{(R_\lambda+h)^2}\dfrac{\partial R_\lambda}{\partial\phi} & 0 & \dfrac{v_E\tan\phi}{(R_\lambda+h)^2} \end{bmatrix} \tag{101a}$$

$$\frac{\partial\boldsymbol{\omega}^N_{N/I}}{\partial\mathbf{v}^N} = \begin{bmatrix} 0 & \dfrac{1}{R_\lambda+h} & 0 \\ -\dfrac{1}{R_\phi+h} & 0 & 0 \\ 0 & -\dfrac{\tan\phi}{R_\lambda+h} & 0 \end{bmatrix} \tag{101b}$$

with

$$\frac{\partial R_\lambda}{\partial\phi} = \frac{a\,e^2\sin\phi\cos\phi}{(1-e^2\sin^2\phi)^{3/2}} \tag{102a}$$

$$\frac{\partial R_\phi}{\partial\phi} = \frac{3a(1-e^2)e^2\sin\phi\cos\phi}{(1-e^2\sin^2\phi)^{5/2}} \tag{102b}$$

The position partials are given by

$$\frac{\partial\dot{\mathbf{p}}^N}{\partial\mathbf{p}^N} = \begin{bmatrix} -\dfrac{v_N}{(R_\phi+h)^2}\dfrac{\partial R_\phi}{\partial\phi} & 0 & -\dfrac{v_N}{(R_\phi+h)^2} \\ -\dfrac{v_E\sec\phi}{(R_\lambda+h)^2}\dfrac{\partial R_\lambda}{\partial\phi} + \dfrac{v_E\sec\phi\tan\phi}{R_\lambda+h} & 0 & -\dfrac{v_E\sec\phi}{(R_\lambda+h)^2} \\ 0 & 0 & 0 \end{bmatrix} \tag{103a}$$

$$\frac{\partial \dot{\mathbf{p}}^N}{\partial \mathbf{v}^N} = \begin{bmatrix} \dfrac{1}{R_\phi + h} & 0 & 0 \\ 0 & \dfrac{\sec\phi}{R_\lambda + h} & 0 \\ 0 & 0 & -1 \end{bmatrix} \tag{103b}$$

The velocity partials are given by

$$\frac{\partial \dot{\mathbf{v}}^N}{\partial \mathbf{p}^N} = \begin{bmatrix} Y_{11} & 0 & Y_{13} \\ Y_{21} & 0 & Y_{23} \\ Y_{31} & 0 & Y_{33} \end{bmatrix}, \quad \frac{\partial \dot{\mathbf{v}}^N}{\partial \mathbf{v}^N} = \begin{bmatrix} Z_{11} & Z_{12} & Z_{13} \\ Z_{21} & Z_{22} & Z_{23} \\ Z_{31} & Z_{32} & 0 \end{bmatrix} \tag{104}$$

where

$$Y_{11} = -\frac{v_E^2 \sec^2\phi}{R_\lambda + h} + \frac{v_E^2 \tan\phi}{(R_\lambda + h)^2}\frac{\partial R_\lambda}{\partial \phi} - 2\omega_e v_E \cos\phi - \frac{v_N v_D}{(R_\phi + h)^2}\frac{\partial R_\phi}{\partial \phi} \tag{105a}$$

$$Y_{13} = \frac{v_E^2 \tan\phi}{(R_\lambda + h)^2} - \frac{v_N v_D}{(R_\phi + h)^2} \tag{105b}$$

$$\begin{aligned} Y_{21} = {} & \frac{v_E\, v_N \sec^2\phi}{R_\lambda + h} - \frac{v_E\, v_N \tan\phi}{(R_\lambda + h)^2}\frac{\partial R_\lambda}{\partial \phi} + 2\omega_e v_N \cos\phi \\ & - \frac{v_E\, v_D}{(R_\lambda + h)^2}\frac{\partial R_\lambda}{\partial \phi} - 2\omega_e v_D \sin\phi \end{aligned} \tag{105c}$$

$$Y_{23} = -v_E\left[\frac{v_N \tan\phi + v_D}{(R_\lambda + h)^2}\right] \tag{105d}$$

$$Y_{31} = \frac{v_E^2}{(R_\lambda + h)^2}\frac{\partial R_\lambda}{\partial \phi} + \frac{v_N^2}{(R_\phi + h)^2}\frac{\partial R_\phi}{\partial \phi} + 2\omega_e v_E \sin\phi + \frac{\partial g}{\partial \phi} \tag{105e}$$

$$Y_{33} = \frac{v_E^2}{(R_\lambda + h)^2} + \frac{v_N^2}{(R_\phi + h)^2} + \frac{\partial g}{\partial h} \tag{105f}$$

and

$$Z_{11} = \frac{v_D}{R_\phi + h}, \quad Z_{12} = -\frac{2v_E \tan\phi}{R_\lambda + h} - 2\omega_e \sin\phi, \quad Z_{13} = \frac{v_N}{R_\phi + h} \tag{106a}$$

$$Z_{21} = \frac{v_E \tan\phi}{R_\lambda + h} + 2\omega_e \sin\phi, \quad Z_{22} = \frac{v_D + v_N \tan\phi}{R_\lambda + h}, \quad Z_{23} = \frac{v_E}{R_\lambda + h} + 2\omega_e \cos\phi \tag{106b}$$

$$Z_{31} = -\frac{2v_N}{R_\phi + h}, \quad Z_{32} = -\frac{2v_E}{R_\lambda + h} - 2\omega_e \cos\phi \tag{106c}$$

with

$$\begin{aligned} \frac{\partial g}{\partial \phi} = {} & 9.780327[1.06048 \times 10^{-2} \sin\phi\cos\phi \\ & - 4.64 \times 10^{-5}(\sin\phi\cos^3\phi - \sin^3\phi\cos\phi)] + 8.8 \times 10^{-9} h\, \sin\phi\cos\phi \end{aligned} \tag{107a}$$

$$\frac{\partial g}{\partial h} = -3.0877 \times 10^{-6} + 4.4 \times 10^{-9}\sin^2\phi + 1.44 \times 10^{-13} h \tag{107b}$$

The matrix G_a is given by

$$G_a = \begin{bmatrix} -\frac{1}{2}\Xi(\hat{\mathbf{q}})(I_{3\times3} - \hat{\mathcal{K}}_g) & 0_{4\times3} & 0_{4\times3} & 0_{4\times3} \\ 0_{3\times3} & 0_{3\times3} & 0_{3\times3} & 0_{3\times3} \\ 0_{3\times3} & 0_{3\times3} & -A_B^N(\hat{\mathbf{q}})(I_{3\times3} - \hat{\mathcal{K}}_a) & 0_{3\times3} \\ 0_{3\times3} & I_{3\times3} & 0_{3\times3} & 0_{3\times3} \\ 0_{3\times3} & 0_{3\times3} & 0_{3\times3} & I_{3\times3} \\ 0_{3\times3} & 0_{3\times3} & 0_{3\times3} & 0_{3\times3} \\ 0_{3\times3} & 0_{3\times3} & 0_{3\times3} & 0_{3\times3} \end{bmatrix} \tag{108}$$

The matrices C and $\dot{C}$ are given by

$$C = \begin{bmatrix} \frac{1}{2}\Xi(\hat{\mathbf{q}}) & 0_{4\times3} & 0_{4\times3} & 0_{4\times3} & 0_{4\times3} & 0_{4\times3} & 0_{4\times3} \\ 0_{3\times3} & I_{3\times3} & 0_{3\times3} & 0_{3\times3} & 0_{3\times3} & 0_{3\times3} & 0_{3\times3} \\ -[\hat{\mathbf{v}}^N\times]A_B^N(\hat{\mathbf{q}}) & 0_{3\times3} & I_{3\times3} & 0_{3\times3} & 0_{3\times3} & 0_{3\times3} & 0_{3\times3} \\ [\hat{\boldsymbol{\beta}}_g\times] & 0_{3\times3} & 0_{3\times3} & I_{3\times3} & 0_{3\times3} & 0_{3\times3} & 0_{3\times3} \\ [\hat{\boldsymbol{\beta}}_a\times] & 0_{3\times3} & 0_{3\times3} & 0_{3\times3} & I_{3\times3} & 0_{3\times3} & 0_{3\times3} \\ [\hat{\mathbf{k}}_g\times] & 0_{3\times3} & 0_{3\times3} & 0_{3\times3} & 0_{3\times3} & I_{3\times3} & 0_{3\times3} \\ [\hat{\mathbf{k}}_a\times] & 0_{3\times3} & 0_{3\times3} & 0_{3\times3} & 0_{3\times3} & 0_{3\times3} & I_{3\times3} \end{bmatrix} \tag{109a}$$

$$\dot{C} = \begin{bmatrix} \frac{1}{4}\Omega(\hat{\boldsymbol{\omega}}_{B/N}^B)\Xi(\hat{\mathbf{q}}) + \frac{1}{2}\Xi(\hat{\mathbf{q}})[\hat{\boldsymbol{\omega}}_{B/N}^B\times] & 0_{4\times3} & 0_{4\times3} & 0_{4\times3} & 0_{4\times3} & 0_{4\times3} & 0_{4\times3} \\ 0_{3\times3} & 0_{3\times3} & 0_{3\times3} & 0_{3\times3} & 0_{3\times3} & 0_{3\times3} & 0_{3\times3} \\ -[\dot{\hat{\mathbf{v}}}^N\times]A_B^N(\hat{\mathbf{q}}) - [\hat{\mathbf{v}}^N\times]A_B^N(\hat{\mathbf{q}})[\hat{\boldsymbol{\omega}}_{B/N}^B\times] & 0_{3\times3} & 0_{3\times3} & 0_{3\times3} & 0_{3\times3} & 0_{3\times3} & 0_{3\times3} \\ 0_{3\times3} & 0_{3\times3} & 0_{3\times3} & 0_{3\times3} & 0_{3\times3} & 0_{3\times3} & 0_{3\times3} \\ 0_{3\times3} & 0_{3\times3} & 0_{3\times3} & 0_{3\times3} & 0_{3\times3} & 0_{3\times3} & 0_{3\times3} \\ 0_{3\times3} & 0_{3\times3} & 0_{3\times3} & 0_{3\times3} & 0_{3\times3} & 0_{3\times3} & 0_{3\times3} \\ 0_{3\times3} & 0_{3\times3} & 0_{3\times3} & 0_{3\times3} & 0_{3\times3} & 0_{3\times3} & 0_{3\times3} \end{bmatrix} \tag{109b}$$

Finally, the Q matrix is given by Eq. (71b).

VII. Simulation Results

In this section simulation results comparing the MEKF and the GEKF are discussed for both the ECEF and NED navigation frames. The gyro and accelerometer measurements are available at 10 Hz and GPS measurements are also available for updates at 10 Hz. Models for these measurements are given in Ref. [5] and Ref. [19] respectively. The total simulation time is 1800 seconds. The rotational rate profile is given 5 deg/min rotation about the x, y, and z axes for the entire simulation. There is also a constant acceleration of 0.1 m/sec^2 about the x and y axes and 0.01 m/sec^2 about the z axis for the entire simulation. The gyro noise parameters are given by $\sigma_{gv} = \sqrt{10}\times10^{-7}$ rad/sec$^{1/2}$ and $\sigma_{gu} = \sqrt{10}\times10^{-10}$ rad/sec$^{3/2}$. The accelerometer parameters are given by $\sigma_{av} = 9.8100\times10^{-7}$ m/sec$^{3/2}$ and $\sigma_{au} = 6.000\times10^{-5}$ m/sec$^{5/2}$. Initial biases for the gyros and accelerometers are given by 0.01 deg/hr and 0.003 m/s^2, respectively, for each axis. The gyro scale factors are $\mathcal{K}_g = 150\times10^{-6}I_{3\times3}$ and $\mathcal{K}_a = 500\times10^{-6}I_{3\times3}$. The initial vehicle position is specified in NED coordinates as $\lambda_0 = 38.4°$, $\Phi_0 = -76.5°$, and $h_0 = 244$ meters.

The results for the ECEF coordinate frame can be seen in Figure 2. The attitude errors for the GEKF and the MEKF are illustrated in Figure 2(a) and Figure 2(b), respectively. Both converge and stay within the 3σ bounds, and it can be seen that there are no differences between the GEKF and MEKF attitude errors. Figures 2(c) and 2(d) show the results for the position error associate with each filter. Both the GEKF and MEKF stay within the 3σ bounds. The velocity errors are shown in Figures 2(e) and 2(f). The GEKF errors appear larger than the MEKF errors, but this is not completely an apples-to-apples comparison. It is argued here that the errors defined by the GEKF are the *correct* errors because they are frame consistent, unlike the MEKF.

Results for the NED coordinate frame can be seen in Figure 3. Figure 3(a) shows the same convergence properties of the GEKF filter when compared to the MEKF in Figure 3(b). This is also true for the position errors in Figures 3(c) and 3(d). The velocity for the NED frame converges for both the GEKF and MEKF, and the errors for both stay within their respective bounds. In Figure 3(e) it is again shown that the error bounds do not decrease to the same level as the MEKF in Figure 3(f). This is because the errors associated with the GEKF are in the consistent frame based on the new error definition.

The next simulation tests the convergence properties of both filters for the NED case. The simulation is run again, but 10 degrees of error are introduced in the initial attitude estimates for both the MEKF and GEKF. The attitude covariance for each filter is now increased to a 3σ bound of 10 degrees for each axis. The rest of the simulation parameters are the same as before. Plots of the attitude errors for both filters are shown in Figure 4. For this case the GEKF shows superior convergence properties over the MEKF. Although not shown here for brevity, this is most likely due to the appearance of coupling terms in the linearized GEKF state-error matrix over the linearized MEKF state-error matrix. These coupling terms

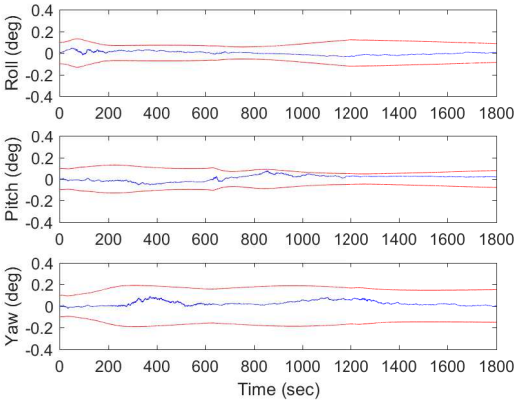

(a) **GEKF Attitude Errors**

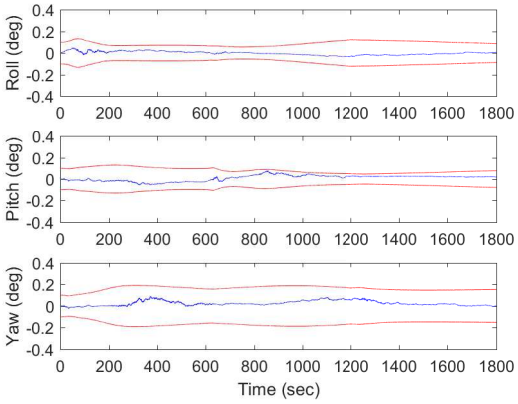

(b) **MEKF Attitude Errors**

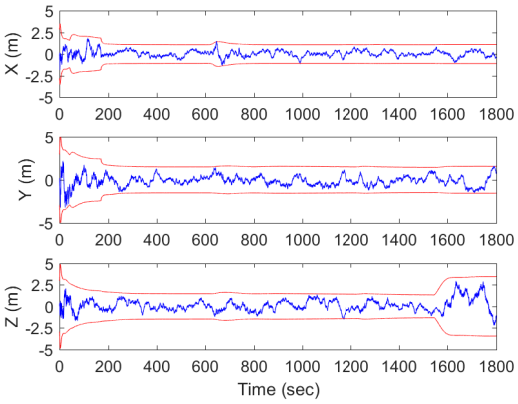

(c) **GEKF Position Errors**

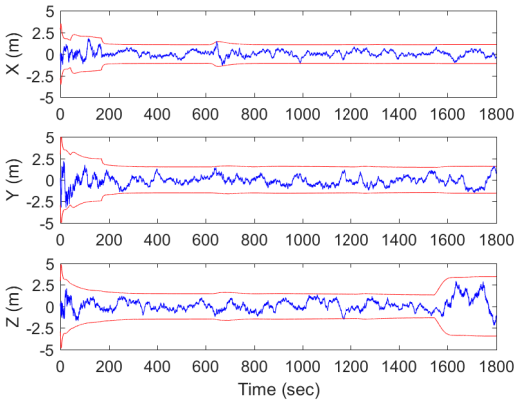

(d) **MEKF Position Errors**

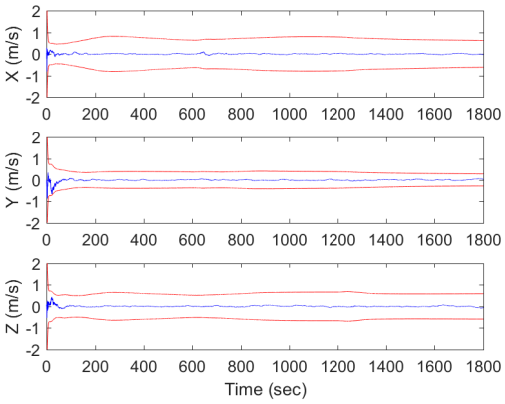

(e) **GEKF Velocity Errors**

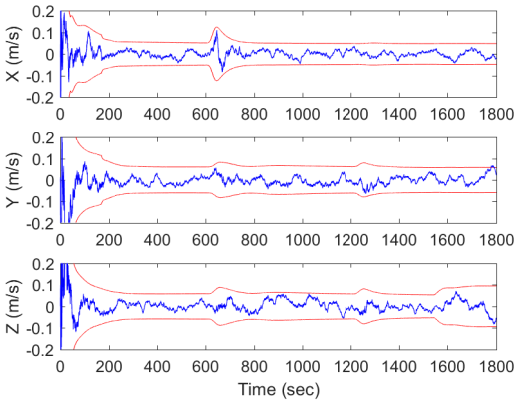

(f) **MEKF Velocity Errors**

Figure 2. Comparison of MEKF and GEKF for ECEF Frame

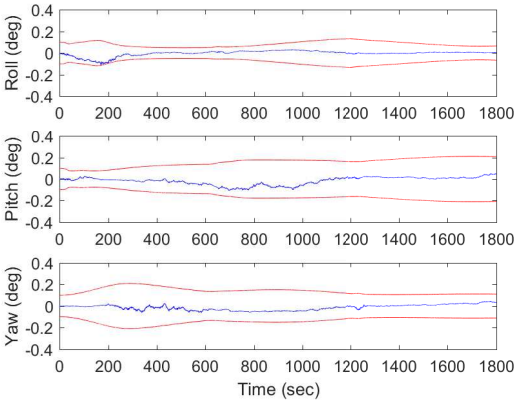

(a) **GEKF Attitude Errors**

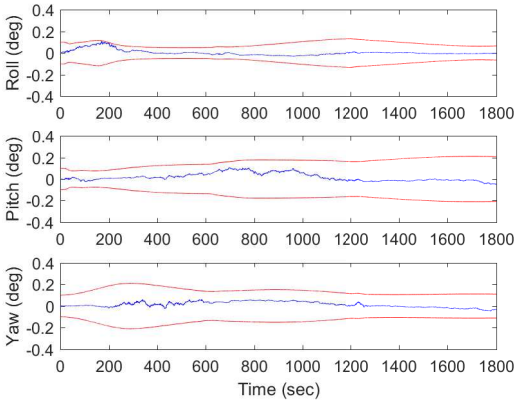

(b) **MEKF Attitude Errors**

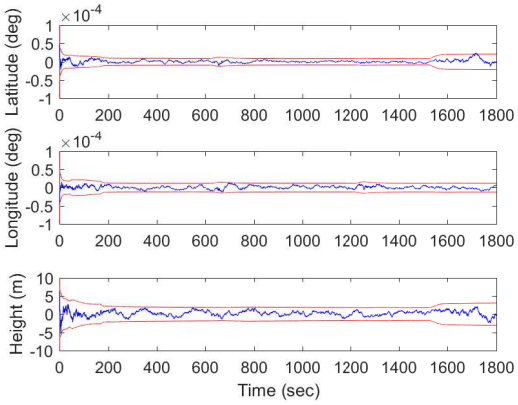

(c) **GEKF Position Errors**

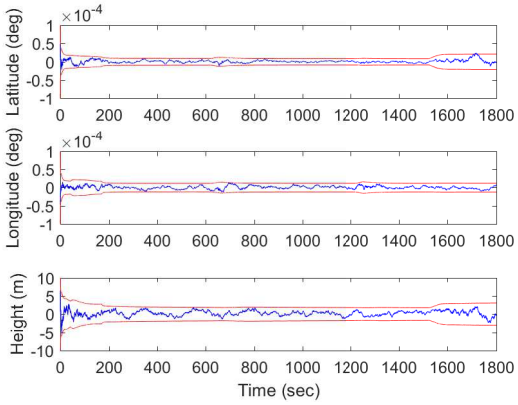

(d) **MEKF Position Errors**

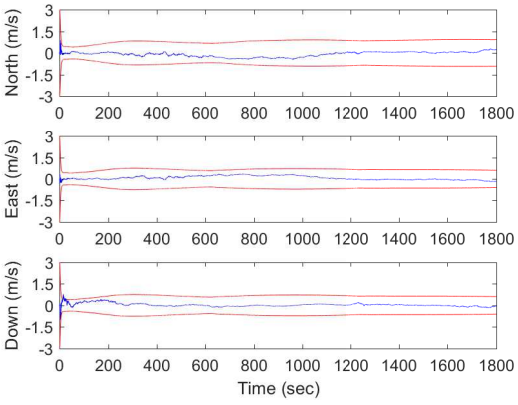

(e) **GEKF Velocity Errors**

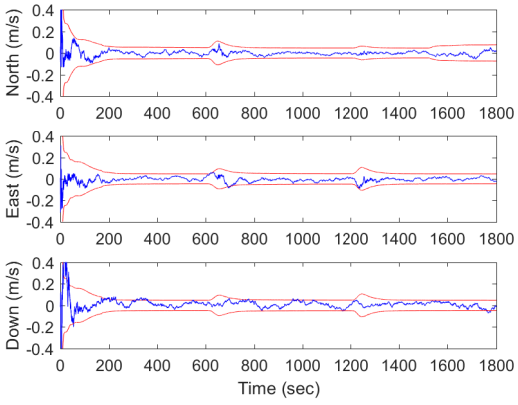

(f) **MEKF Velocity Errors**

Figure 3. Comparison of MEKF and GEKF for NED Frame

appear because of transport terms that exist in the GEKF in order to obtain frame-consistent errors. As noted earlier, the GEKF errors are frame consistent, which represent the actual real-world errors over the MEKF. This is arguably more important since in practice the accuracy of an estimate is not known and the error bounds is the primary metric of confidence. This can improve upon other aspects such as control, data association, tracking performance, to name a few.

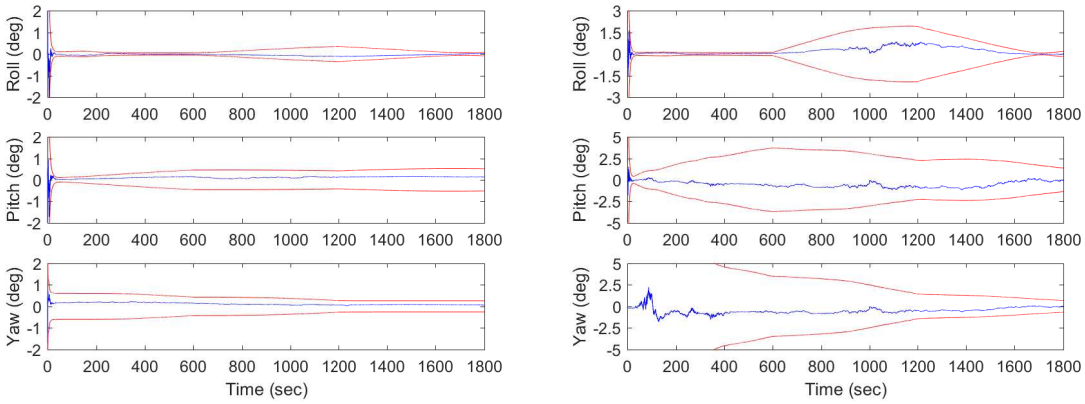

(a) **GEKF Attitude Errors** (b) **MEKF Attitude Errors**

Figure 4. Comparison of MEKF and GEKF for NED Frame with Large Initial Attitude Errors

VIII. Conclusions

A new error-representation was presented in this paper for inertial navigation applications. The error-representation is frame consistent for both body-frame and reference-frame errors. A direct relationship between these two frames shows that even though the error-kinematics are different for the body and reference frames only one error-kinematics needs to be used in the filter design. Here the body-frame error-kinematics is used, which is typically used in standard inertial navigation filters. The geometric-based Kalman filter shows that more coupling effects exist in the state-error dynamics, which leads to better convergence properties than the standard inertial navigation Kalman filter when large initial condition errors are present. Also, the reference errors in the geometric-based Kalman filter are different than the standard inertial navigation Kalman filter, which is important when overall control performance is evaluated.

Acknowledgements

Special thanks to F. Landis Markley of NASA Goddard Space Flight Center, and Michael S. Andrle of MIT Lincoln Laboratory for their contributions, discussions and comments which played a critical role in the development and presentation of this work.

References

[1]Wrigley, W., "History of Inertial Navigation," *Navigation, Journal of the Institute of Navigation*, Vol. 24, No. 1, Spring 1977, pp. 1–6, doi:10.1002/j.2161-4296.1977.tb01262.x.

[2]Savage, P. G., "Blazing Gyros: The Evolution of Strapdown Inertial Navigation Technology for Aircraft," *Journal of Guidance, Control, and Dynamics*, Vol. 36, No. 3, May-June 2013, pp. 637–655, doi:10.2514/1.60211.

[3]Miller, P. A., Farrell, J. A., Zhao, Y., and Djapic, V., "Autonomous Underwater Vehicle Navigation," *IEEE Journal of Oceanic Engineering*, Vol. 35, No. 3, July 2010, pp. 663–678, doi:10.1109/JOE.2010.2052691.

[4]Barshan, B. and Durrant-Whyte, H. F., "Inertial Navigation Systems for Mobile Robots," *IEEE Transactions on Robotics and Automation*, Vol. 11, No. 3, June 1995, pp. 328–342, doi:10.1109/70.388775.

[5]Markley, F. L. and Crassidis, J. L., *Fundamentals of Spacecraft Attitude Determination and Control*, chap. 3,6, Springer,

New York, NY, 2014, pp. 147, 245–246, 353–358, doi:10.1007/978-1-4939-0802-8.

[6]Kalman, R. E. and Busy, R. S., "New Results in Linear Filtering and Prediction Theory," *Journal of Basic Engineering*, Vol. 83, No. 1, March 1961, pp. 95–108, doi:10.1115/1.3658902.

[7]Grewal, M. S. and Andrews, A. P., "Applications of Kalman Filtering in Aerospace 1960 to the Present," *IEEE Control Systems*, Vol. 30, No. 3, June 2010, pp. 69–78, doi:10.1109/MCS.2010.936465.

[8]Stuelpnagel, J., "On the Parametrization of the Three-Dimensional Rotation Group," *SIAM Review*, Vol. 6, No. 4, Oct. 1964, pp. 422–430, doi:10.2307/2027966.

[9]Shuster, M. D., "A Survey of Attitude Representations," *Journal of the Astronautical Sciences*, Vol. 41, No. 4, Oct.-Dec. 1993, pp. 439–517.

[10]Lefferts, E. J., Markley, F. L., and Shuster, M. D., "Kalman Filtering for Spacecraft Attitude Estimation," *Journal of Guidance, Control, and Dynamics*, Vol. 5, No. 5, Sept.-Oct. 1982, pp. 417–429, doi:10.2514/3.56190.

[11]Crassidis, J. L., "Sigma-Point Kalman Filtering for Integrated GPS and Inertial Navigation," *IEEE Transactions on Aerospace and Electronic Systems*, Vol. 42, No. 2, June 2006, pp. 750–756, doi:10.1109/TAES.2006.1642588.

[12]Cheng, Y. and Crassidis, J. L., "Particle Filtering for Attitude Estimation Using a Minimal Local-Error Representation," *Journal of Guidance, Control, and Dynamics*, Vol. 33, No. 4, July-Aug. 2010, pp. 1305–1310, doi:10.2514/1.47236.

[13]Crassidis, J. L., Markley, F. L., and Cheng, Y., "Survey of Nonlinear Attitude Estimation Methods," *Journal of Guidance, Control, and Dynamics*, Vol. 30, No. 1, Jan.-Feb. 2007, pp. 12–28, doi:10.2514/1.22452.

[14]Tang, Y., Wu, Y., Wu, M., Wu, W., Hu, X., and Shen, L., "INS/GPS Integration: Global Observability Analysis," *IEEE Transactions on Vehicular Technology*, Vol. 58, No. 3, March 2009, pp. 1129–1142, doi:10.1109/TVT.2008.926213.

[15]Andrle, M. S. and Crassidis, J. L., "Attitude Estimation Employing Common Frame Error Representations," *Journal of Guidance, Control, and Dynamics*, Vol. 38, No. 9, Sept. 2015, pp. 1614–1624, doi:10.2514/1.G001025.

[16]Farrell, J. and Barth, M., *The Global Positioning System & Inertial Navigation*, chap. 2, McGraw-Hill, New York, NY, 1998.

[17]Vallado, D. A. and McClain, W. D., *Fundamentals of Astrodynamics and Applications, 4th Edition*, Microcosm Press, Hawthorne, CA, 2013, pp. 182–184.

[18]Sofair, I., "Improved Method for Calculating Exact Geodetic Latitude and Altitude Revisited," *Journal of Guidance, Control, and Dynamics*, Vol. 23, No. 2, March-April 2000, pp. 369, doi:10.2514/2.4534.

[19]Crassidis, J. L. and Junkins, J. L., *Optimal Estimation of Dynamic Systems, 2nd Edition*, CRC Press, Boca Raton, FL, 2012, pp. 452–453, 466–475.

[20]Gai, E., Daly, K., Harrison, J., and Lemos, L., "Star-Sensor-Based Attiude/Attitude Rate Estimator," *Journal of Guidance, Control, and Dynamics*, Vol. 8, No. 5, Sept.-Oct. 1985, pp. 560–565, doi:10.2514/3.56393.

[21]Tanygin, S., "Projective Geometry of Attitude Parameterizations with Applications to Control," *Journal of Guidance, Control and Dynamics*, Vol. 36, No. 3, May-June 2013, pp. 656–666, doi:10.2514/1.60081.

[22]Jekeli, C., *Inertial Navigation Systems with Geodetic Applications*, chap. 4, Walter de Gruyter, Berlin, Germany, 2000.